Simultaneous Process Synthesis and Control Design under Uncertainty: A Worst-Case Performance Approach

Kelvyn Sánchez-Sánchez and Luis Ricardez-Sandoval
Dept. of Chemical Engineering, University of Waterloo, Waterloo, Ontario N2L 3G1 Canada

DOI 10.1002/aic.14040
Published online April 12, 2013 in Wiley Online Library (wileyonlinelibrary.com)

A new methodology that includes process synthesis and control structure decisions for the optimal process and control design of dynamic systems under uncertainty is presented. The method integrates dynamic flexibility and dynamic feasibility in a single optimization formulation, thus, reducing the costs to assess the optimal design. A robust stability test is also included in the proposed method to ensure that the optimal design is stable in the presence of magnitude-bounded perturbations. Since disturbances are treated as stochastic time-discrete unmeasured inputs, the optimal process synthesis and control design specified by this method remains feasible and stable in the presence of the most critical realizations in the disturbances. The proposed methodology has been applied to simultaneously design and control a system of CSTRs and a ternary distillation column. A study on the computational costs associated with this method is presented and compared to that required by a dynamic optimization-based scheme. © 2013 American Institute of Chemical Engineers *AIChE J*, 59: 2497–2514, 2013

Keywords: simultaneous design and control, mixed-integer nonlinear optimization, process synthesis, control structure selection, robust control theory

Introduction

Current trends in global economy are driving industries to produce high-quality products that can meet the clients' demands at minimum cost and under stringent operational, environmental and safety restrictions. Optimal process design represents an attractive alternative to specify highly efficient and integrated processes that can meet the production targets and minimize product variability in the presence of external disturbances and uncertainty in physical parameters. Process synthesis analysis is one of the first tasks that needs to be performed in process design and is aimed to specify, from a given set of process flow sheets, the most suitable and economically attractive process layout that can meet the design goals. This activity has been traditionally performed using process heuristics or from previous experience with similar processes.[1] Steady-state process simulators such as Aspen Plus or PRO/II are extensively used at this stage of the design to determine the most suitable process flow sheet that can meet the production targets at a nominal (steady-state) condition. Alternatively, a large-scale mixed-integer nonlinear optimization problem (MINLP) can be formulated to obtain an optimal process flow sheet at steady-state. In addition, uncertainty in the physical model parameters can be added to the formulation to obtain an optimal steady-state process design under uncertainty.[2] Once the process flow sheet and the corresponding capacities of the key process units has been specified, the process dynamics, the effect of external perturbations to products variability and the compliance with the process constraints are considered in the design. That is, dynamic flexibility and dynamic feasibility analyses are performed on the optimal steady-state process design. It is often found that the process design specifications, e.g., the process flow sheet and the corresponding sizes for the equipment, imposes a limitation on the dynamic operability of the process[3] or it may produce violations to key process, safety or environmental constraints. Although safety overdesign factors can be added to the process units' sizes to accommodate product variability, this relaxation often leads to the specification of expensive designs. Moreover, studies have shown that the optimal steady-state process design may return processes that are dynamically unfeasible, i.e., the system cannot be operated in the transient domain.[4,5]

Based on the aforementioned, there is a motivation to consider the dynamic operability of the process in the early stages of the design since the transient operation of the process is largely affected by the specification of the process flow sheet (process synthesis analysis) and the corresponding process units' capacities. *Integration of process and control design* is becoming a widely accepted approach in both academia and industry. The key idea in integration of process design and control, also referred to as *simultaneous design and control*, is to obtain the optimal process design while considering the steady-state and the dynamic operation of the process in the presence of variability in the disturbances and uncertainty in the physical parameters of the process. Several approaches have been proposed to assess optimal process and control design. Due to computational limitations,

Additional Supporting Information may be found in the online version of this article.

Correspondence concerning this article should be addressed to L. Ricardez-Sandoval at laricard@uwaterloo.ca.

the first methodologies proposed in this field described the behavior of the process using steady-state models or linear dynamic models and made used of open-loop controllability metrics to measure the performance of the system.[3,6–8] Only a few of these controllability index-based methodologies accounted for structural changes in the process flow sheet,[9,10] or incorporated advanced control techniques within the analysis, e.g., model predictive control.[11] Advances in computational sciences enabled the development of comprehensive integration of design and control methodologies based on dynamic optimization algorithms.[12–21] Dynamic optimization-based methodologies are usually formulated as a two-stage iterative decomposition algorithm. In the first stage, the optimal process design and control configuration that meets the process constraints at minimum cost in the presence of specific (critical) realizations in an uncertain process disturbance function is obtained. The disturbance function is a time-dependent function that includes uncertain (critical) model parameters. This stage, usually referred to as a *dynamic flexibility analysis*, is usually formulated as a multiperiod MINLP. In the second stage, a *dynamic feasibility analysis* is performed on the optimal design obtained from the previous stage and is aimed to identify the critical realizations in the uncertain disturbance function that produce process constraint violations during the dynamic operation of the process. If process constraints are exceeded, then a new dynamic flexibility analysis must be performed using the critical realizations in the process disturbances identified in the dynamic feasibility test. This algorithm continues up until no process constraints violations are observed in the dynamic feasibility analysis. Methodologies based on dynamic metrics computed from robust control theory,[22–28] normal vectors on critical manifolds[29–31] and probability-based methods[32] have also been reported in the literature. Moreover, systematic methods that apply process heuristics for process synthesis analysis and reverse design algorithms have been proposed for simultaneous of design and control.[33–35] Furthermore, the implementation of advanced control techniques such as model predictive control (MPC) within the integration of design and control framework are also available.[36–40] An in-depth review of the current approaches available for optimal process and control design is available elsewhere.[41–43]

The aim of this article is to present a new methodology for simultaneous process synthesis and control structure design. In the proposed approach, dynamic flexibility and dynamic feasibility are evaluated simultaneously, i.e., a single-optimization formulation is proposed to evaluate dynamic flexibility and feasibility. Thus, this method does not require a decomposition strategy as needed by the current dynamic optimization-based methods.[12–16,37,44] Likewise, this methodology obtains an optimal design that is feasible in the presence of the most critical time-discrete realizations in the disturbances. That is, this methodology does not make any assumptions about the disturbances' dynamics, i.e., it treats disturbances as stochastic bounded perturbations. To the authors' knowledge, this is the first method that proposes a formulation for optimal process synthesis and control structure selection that simultaneously evaluates dynamic flexibility and dynamic feasibility in the presence of the worst-case (critical) time-trajectories in the disturbances. Moreover, process stability is fundamental to ensure the safe operation of a system in the presence of disturbances. In this work, a formal robust stability test is included in this method to ensure the process asymptotic stability in the presence of bounded disturbances. The proposed simultaneous design and control methodology was tested using a system of CSTRs and a ternary distillation column system. These case studies were also used to investigate the computational costs associated with this method.

The new algorithmic framework follows the work proposed by the corresponding author[23,45,46] that aimed to address the simultaneous process and control design of systems with fixed process flow sheet and control structure. In this method, structural decisions are explicitly included in the analysis by proposing a new two-stage strategy for optimal process synthesis and control structure design. In this algorithm, the applicability of the worst-case performance tool presented in[45–56] is extended for process synthesis and control structure selection by embedding the tool within a new formulation that evaluates the system's dynamic flexibility and feasibility simultaneously (Stage 1 in the proposed algorithm). As shown in the first case study presented in this work, suboptimal designs can be obtained when process synthesis and control structure decisions are not formally included in the analysis. Moreover, a computational efficient method is presented here to compute the multiple critical realizations in the disturbances simultaneously using computer parallelization techniques. Furthermore, a rigorous robust stability analysis is formally included in this approach (Stage 2 in the proposed algorithm) to ensure that the process synthesis and control structure design obtained by this method remains feasible and asymptotically stable under the effect of bounded disturbances.

This article is structured as follows: the next section presents the formulation proposed in this work for optimal process synthesis and control design. The implementation of this approach is illustrated in the section entitled: Case Study 1 using a system of CSTRs connected in series. In the section entitled: Case Study 2, the simultaneous design and control of a ternary distillation system using this methodology is presented. A study on the computational costs associated with this approach and comparisons with a formal dynamic optimization based method is presented in the section. Concluding remarks are presented at the end of this article.

Mathematical Framework

This section presents the methodology proposed for optimal process synthesis and control structure design. A brief description of the tool used to calculate the worst-case output performance is presented next. Then, the formulation proposed for the simultaneous evaluation of dynamic flexibility and feasibility is described. The robust asymptotic stability test is presented at the end of this section.

Worst-case performance tool

The method used to specify the disturbances is central in any optimization-based simultaneous design and control method since it largely determines the approach used to assess the optimal design. In this work, the disturbances are defined as follows

$$\begin{aligned} &\mathbf{d}=\left\{\mathbf{d}_1(t),...,\mathbf{d}_q(t),...,\mathbf{d}_{nq}(t)\right\} \\ &\mathbf{d}_q(t)\approx\left\{d_q(i)|d_q^{low}\le d(i)\le d_q^{up}\right\} \\ &t=i\Delta t;\qquad i=0,1,...,m \end{aligned} \tag{1}$$

where the time vector t has been discretized to reduce $\mathbf{d}\in\Re^{n_d}$ into a finite set; hence, $\mathbf{d}_q(t)$ is approximated to a finite

set of m piecewise constant realizations of the q^{th} disturbance propagated through time; i and Δt in (1) are the sampling time and the sampling interval, respectively. $\mathbf{d}_q(t)$ can be reformulated as an uncertain parameter as follows

$$\mathbf{d}_q = d_{nom,q} \pm \delta d_q$$
$$d_{nom,q} = \frac{d_q^{up} + d_q^{low}}{2}; \qquad \delta d_q = \frac{d_q^{up} - d_q^{low}}{2} \tag{2}$$

where $d_{nom,q}$ and δd_q are the nominal (steady-state) value and the largest deviation expected for the q^{th} disturbance, respectively. Thus, $\mathbf{d}_q$ can take on values that satisfy description (2) at any time interval i. Description (2) can be extended to the rest of the disturbances included in $\mathbf{d}$. As shown in (1) d_q^{up}, d_q^{low}, Δt and m are the specifications needed to describe $\mathbf{d}_q$. Note that the dependence of $\mathbf{d}_q$ on t in (2) was dropped to simplify notation. Also, note that the description for $\mathbf{d}_q$ in (2) is not limited to follow a user-defined function as it is proposed in previous methods that included process synthesis and control structure design.[12–14,16–21,37] The approach proposed here aims to address that limitation by searching for the optimal process synthesis and control design that can accommodate the critical time-discrete realizations in the disturbances that comply with (2), i.e., this method searches for the critical realizations in the disturbances that produces the worst-case increase (or decrease) in the process outputs, i.e., *the worst-case performance*. The worst-case performance tool used in this work has been considered in previous methods that did not include structural decisions in the analysis.[23,45,46] This work extends and improves the applicability of that tool by adding process synthesis and control structure decisions within the formulation and by presenting a new parallel algorithm that enables the efficient evaluation of the worst-case performance. As shown in the first case study, process flow sheet decisions are essential to specify optimal process designs. Moreover, the parallel algorithm proposed in this work reduces significantly the computational costs associated with this method (see the computational performance section). A brief description of worst-case performance tool is presented next; a detailed description of the worst-case performance tool is given in[45,46].

In the worst-case performance method, the closed-loop nonlinear dynamic behavior of the process is represented by a finite impulse response model, which model parameters are bounded by upper and lower limits, i.e., an uncertain finite impulse response (UFIR) model. This uncertain model is as follows[45,46]

$$\hat{y}_{q,p}(k+1) = \sum_{i=0}^{N} h_{i,q}(k-i+1) d_q(i) h_{i,q}(k-i+1)$$
$$= \left[\bar{h}_{i,q}(k-i+1) - \delta h_{i,q}(k-i+1), \bar{h}_{i,q}(k-i+1) + \delta h_{i,q}(k-i+1)\right] \tag{3}$$

where $d_q(i)$ is defined in Eqs. 1 and 2; $\hat{y}_q(k+1)$ is the p^{th} output (in deviation form) due to a change in the q^{th} disturbance at the $(k+1)^{th}$ sampling interval. The set $\mathbf{\mathfrak{y}_p} \in \Re^{n_d}$, contains the individual UFIR models that describe the dynamics between each disturbance included in $\mathbf{d}$ and the output p around a nominal operating state specified by $\boldsymbol{\xi}$. $h_{i,q}(k\text{-}i+1)$ is the uncertain impulse response model parameter at the $(k\text{-}i+1)^{th}$ sampling interval. As shown in (3), $h_{i,q}(k\text{-}i+1)$ is defined in terms of $\bar{h}_{i,q}(k-i+1)$ and $\delta h_{i,q}(k-i+1)$, which are the nominal value and the uncertainty associated with the impulse response coefficient. As shown in (3), $h_{i,q}(k\text{-}i+1)$ can take on values that are bounded by the interval defined by $\bar{h}_{i,q}(k\text{-}i+1)$ and $\delta h_{i,q}(k-i+1)$, respectively. Hence, the UFIR model (3) can be considered as a family of linear impulse response models, each evaluated at a particular combination in the impulse response model coefficients. The uncertain terms $\delta h_{i,q}(k-i+1)$ is used in this method to capture the system's response to changes in the disturbances. That is, these uncertain terms are used to describe the variability in the output that cannot be accurately described using nominal impulse response model coefficients, i.e., using only a linear impulse response model. Accordingly, the uncertain model parameters $\delta h_{i,q}(k-i+1)$, do not represent the uncertainty of an explicit model parameter or neglected dynamics in the actual process model equations. Instead, these uncertain terms are used by the UFIR model to represent the actual nonlinear process model in closed-loop and therefore to account for the nonlinear dynamic behavior of the system due to changes in the disturbances. Note that the only inputs to the UFIR model are the disturbances; thus, model (3) is obtained around a reference state ($\boldsymbol{\xi}$), and it is only valid in the vicinity of that operating state. Assuming n_y process outputs, a total of $n_y n_d$ UFIR models such as (3) need to be identified around ($\boldsymbol{\xi}$) to obtain a complete description of the process model. Each finite impulse response model is expected to capture the process dynamic characteristics between a process output, e.g., p, and a disturbance, e.g., $q, \left(\mathbf{\mathfrak{y}}_{q,p}\right)$. The algorithm proposed in this approach to identify UFIR models is as follows:

1. Define a nominal (steady-state) operating point ($\boldsymbol{\xi}$) at which the finite impulse response model needs to be identified. The operating state $\boldsymbol{\xi}$ is specified by the set of optimization variables included in the optimal process and control design formulation. In addition, define the maximal change expected for each disturbance considered in the analysis, i.e., δd_q, as it is shown in (2).

   For each process output p considered in the analysis:
2. Design an excitation signal, e.g., a white noise signal or a pseudorandom binary signal (PRBS), for the n_d disturbances considered in the analysis. This input signal has to be designed based on the dynamic characteristics of the process in the vicinity of the nominal operating point $\boldsymbol{\xi}$. Guidelines to design meaningful excitation signals are discussed elsewhere.[47]
3. Simulate the closed-loop dynamic behavior of the process using the n_d excitation signals designed for the disturbance set $\mathbf{d}$. As shown in Figure 1, the simulation that describes the variability of a process output due to the changes in the n_d disturbances is performed in tandem, i.e., one excitation disturbance signal is used to simulate the process at a time, while the rest of the disturbances are set to their constant (nominal) values. Then, another excitation disturbance signal is used for simulations, while the other disturbances remain at their nominal value. Although this approach requires additional programming for its implementation, this procedure improves the computational efficiency in the identification stage. As it is discussed in the section entitled: Evaluation of the worst-case performance using a parallel algorithm, the implementation of this procedure enables the simultaneous evaluation of multiple process outputs, which improves the computational efficiency of this method (see the computational performance section).

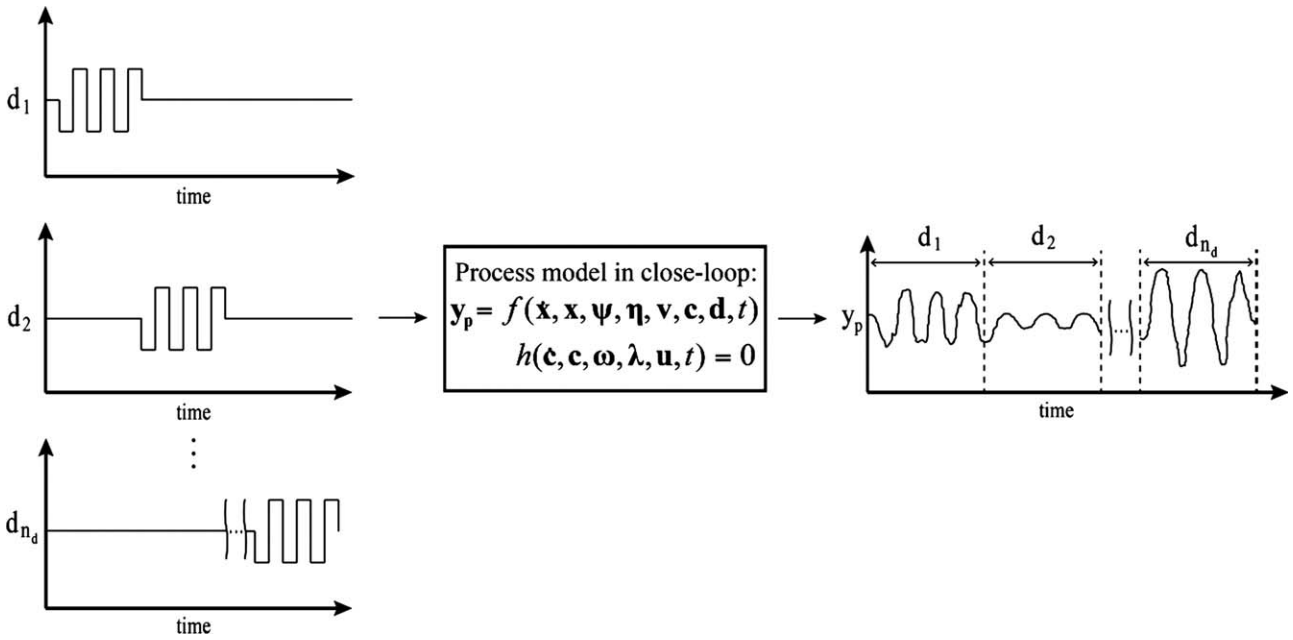

Figure 1. Simulation approach for the identification of UFIR models.

4. As shown in Figure 1, the data set collected from the simulations is subdivided into n_d data arrays; each array contains the response of the p^{th} process output to changes in a specific input disturbance. Each input-output data array is then used to fit a linear impulse response model using standard systems identification techniques such as the least-squares method.[47] The variance in the model parameter estimates, usually specified by the covariance matrix, can be used to represent the uncertainty of each of the model parameters included in the finite impulse response model, i.e., $\boldsymbol{\delta}\mathbf{h}_{i,q}$. Accordingly, this identification test returns n_d UFIR models; each uncertain model is an element in $\hat{\mathbf{y}}_\mathbf{p}$. Each model describes the dynamic behavior between a specific disturbance, e.g., $\mathbf{d_q}$, and the p^{th} output, i.e., $\hat{\mathbf{y}}_{q,p}$.
5. Repeat steps 2–4 up until the n_y outputs considered in the analysis have been evaluated.

The largest variability in $\mathbf{y_p}$ due to changes in $\mathbf{d}$, i.e., the worst-case performance in output p, can be obtained as follows

$$\begin{aligned} &\max_{\mathbf{d}} \|\mathbf{y_p}\|_\infty \\ &s.t. \quad \mathbf{y_p} = f(\dot{\mathbf{x}}, \mathbf{x}, \boldsymbol{\psi}, \boldsymbol{\eta}, \mathbf{v}, \mathbf{c}, \mathbf{d}, t) \\ &\qquad h(\dot{\mathbf{c}}, \mathbf{c}, \boldsymbol{\omega}, \boldsymbol{\lambda}, \mathbf{u}, t) = 0 \\ &\qquad t = [0, t_f) \end{aligned} \tag{4}$$

where the functions f and h represent the process nonlinear model and the controller equations considered in the analysis, respectively. The variable $\mathbf{y_p}$ contains the response of the p^{th} process output to a particular time-discrete realization in $\mathbf{d}$ and is a function of the states of the closed-loop system, i.e., $\mathbf{x}$ and $\mathbf{c}$, the process design variables of type real ($\boldsymbol{\eta}$), the process synthesis or design variables of type integer ($\boldsymbol{\psi}$), the set of binary variables that specifies the control structure ($\boldsymbol{\omega}$), the nominal (steady-state) operating conditions in the process outputs ($\mathbf{v}$), the nominal (steady-state) values in the manipulated variables ($\mathbf{u}$), the controller tuning parameters ($\boldsymbol{\lambda}$), and the disturbances ($\mathbf{d}$) affecting the process. Discretization techniques can be implemented in (4) to reduce this problem into a multiperiod (finite) stochastic optimization problem. Problem (4) assumes that $\boldsymbol{\psi}$, $\boldsymbol{\eta}$, $\boldsymbol{\omega}$, $\mathbf{v}$, $\mathbf{u}$, $\boldsymbol{\lambda}$, remain fixed during the calculations; thus, problem (4) needs to be embedded within another optimization formulation (usually an MINLP) that considers the process design and control decisions as optimization variables. At each iteration step in the outer (MINLP) optimization problem, the worst-case performance for each process output needs to be calculated using problem (4), which is a computationally intensive task. Thus, the implementation of that approach for the optimal process synthesis and control design of large-scale systems may result in prohibitive computational times. The main limitation in (4) is that f is usually described by a set of nonlinear differential equations. On the other hand, the UFIR model (3), which represents the closed-loop process dynamics, i.e., f and h in (4), is linear with respect to the model parameters. Thus, tools from robust control analysis can be used to reformulate problem (4) as a robust formulation that enables the computation of the worst-case performance using uncertain models such as (3). Hence, the worst-case performance output for p around a current state $\boldsymbol{\xi}$, i.e., $\hat{\mathbf{y}}$, can be calculated if (4) is rewritten as a mixed structured singular value problem, i.e.

$$\max_{\mathbf{d}} \|\hat{\mathbf{y}}_\mathbf{p}\|_\infty \quad \leq \quad \gamma^*_{\hat{y}_p} \iff \quad \mu_{\boldsymbol{\Delta}}(\mathbf{M}) - \gamma_{\hat{y}_p} = 0 \tag{5}$$

where $\gamma_{\hat{y}_p}$ is a real positive scalar and $\gamma^*_{\hat{y}_p}$ is the value in $\gamma_{\hat{y}_p}$ that satisfies the equality constraint shown in (5). The scalar $\gamma^*_{\hat{y}_p}$ represents a bound on the worst-case performance on output p due to changes in $\mathbf{d}$. The first term in left-hand-side in the equality constraint in (5) is referred to as the μ-analysis problem, i.e., $\mu_{\boldsymbol{\Delta}}(\mathbf{M})$.[48–50] The two inputs in μ-analysis are the interconnection matrix $\mathbf{M}$ and the perturbation block $\boldsymbol{\Delta}$. The elements of $\mathbf{M}$ are functions of the UFIR model parameters, i.e., $\bar{h}_{i,q}(k-i+1)$ and $\delta h_{i,q}(k-i+1)$, the disturbances $\mathbf{d}$, and the parameter $\gamma_{\hat{y}_p}$, whereas the diagonal elements of $\boldsymbol{\Delta}$ denote the uncertainty associated with realizations in $\mathbf{d}$,

and the uncertainty in the impulse response coefficients. The elements in $\mathbf{\Delta}$ are the unknowns in the μ-analysis calculation.[48–50] The structures of $\mathbf{M}$ and $\mathbf{\Delta}$ are shown online in the supplementary material (Section A). To obtain $\gamma^*_{\hat{y}_p}$ from (5), a numerical method for finding roots needs to be implemented. The method iterates over $\gamma_{\hat{y}_p}$ until a value that satisfies the equality criterion (7) is found, i.e., $\gamma^*_{\hat{y}_p}$. The critical profile on each of the process disturbances that generates the worst-case performance of the output p can be obtained as follows[45,46]

$$\mathbf{d}^*_{\mathbf{p}} = \gamma^*_{\hat{y}_p} \mathbf{M}_{13} \cdot \mathbf{\Delta}^*_d \tag{6}$$

where $\mathbf{M}_{13}$ is an element of matrix $\mathbf{M}$, whereas $\mathbf{\Delta}^*_d$ represents the solution obtained from μ-analysis calculation when $\gamma_{\hat{y}_p} = \gamma^*_{\hat{y}_p}$ (see Eqs. A.2 and A.6 in the supplementary material); $\mathbf{d}^*_{\mathbf{p}}$ contains the time-discrete realizations in the disturbances that produce the worst-case performance for the output p. Hence, the actual worst-case performance in $\hat{\mathbf{y}}(y_{wc,p})$ can be obtained from simulations of the complete mechanistic closed-loop process model, represented by f and h in problem (4), using $\mathbf{d}^*_{\mathbf{p}}$ as input. The equality constraint formulation presented in (5) represents the worst-case performance tool implemented in this work to identify the critical realizations in the disturbances that produces the actual worst-case performance in the process outputs. Note that parametric uncertainty can also be included in this analysis by embedding the structured singular value formulation shown in (5) within an optimization formulation that aims to search for the value in the uncertain parameter that generates the worst-case performance in a process output. Additional remarks regarding the worst-case performance tool are presented online in supplementary material (Section A).

Evaluation of the worst-case performance using a parallel algorithm

The computation of $\gamma^*_{\hat{y}_p}$ and $\mathbf{d}^*_{\mathbf{p}}$ requires the identification of multiple UFIR models around a nominal operating state $\boldsymbol{\xi}$. Hence, the computation of $\gamma^*_{\hat{y}_p}$ and $\mathbf{d}^*_{\mathbf{p}}$ may become intensive depending on the size of the system. Nevertheless, the identification method shown in Figure 1 for the UFIR models enables the simultaneous evaluation of multiple worst-case performance process outputs. Accordingly, the procedure outlined earlier for the identification of the uncertain model (3), and the corresponding computation of $\gamma^*_{\hat{y}_p}$, $\mathbf{d}^*_{\mathbf{p}}$ and $y_{wc,p}$, can be implemented using computer parallelization techniques. Figure 2 presents the algorithm proposed here to perform the simultaneous evaluation of the worst-case performance for n_y outputs. As shown in Figure 2, the computation of the worst-case performance on the process outputs is performed individually using a CPU with multiple cores. The first step in the algorithm is to design $n_d n_y$ excitation signals. Then, the simultaneous identification of n_y UFIR models, each describing the dynamics between the disturbances $\mathbf{d}$ and a given output, e.g., $\hat{\mathbf{y}}_{\mathbf{p}}$, is performed using a CPU with multiple cores. The individual identification of UFIR models for each output is performed following the identification procedure described above, and that is schematically shown in Figure 1. Following Figure 2, bounds on the worst-case performance for each output $\hat{\mathbf{y}}_{\mathbf{p}}$ $\left(\gamma^*_{\hat{y}_p}\right)$, and its corresponding critical time-discrete disturbance profile $\mathbf{d}^*_{\mathbf{p}}$, are calculated simultaneously. The critical disturbance profile obtained for each output $\mathbf{d}^*_{\mathbf{p}}$ is used as an input to simulate the complete closed-loop process model, f and h; these simulations are implemented in parallel since specific critical disturbance profiles are obtained for each output and are independent of each other. Accordingly, the actual worst-case performance for each output is extracted from their corresponding simulations. The computer parallel algorithm presented in Figure 2 can be implemented in MATLAB® using the *parfor* built-in function that executes parallel algorithms on CPUs with multiple cores. The identification method proposed for the UFIR models and the parallel algorithm presented in Figure 2 represent an improvement to the previous methods presented by Ricardez-Sandoval and coworkers[22,23,45,46] since both the identification and computation of the worst-case performance were performed in a serial fashion. Moreover, it can be shown that the corresponding identification of a UFIR model followed by the computation of the critical realization in the disturbances that generates the worst-case performance is much less intensive than the formal computation of the worst-case scenario using problem (4).

Simultaneous dynamic feasibility and flexibility formulation

Figure 3 illustrates the algorithm proposed in this work to attain the optimal process synthesis and control design of dynamic systems in the presence of the critical time-discrete realizations in the disturbances. As shown in that figure, an iterative approach is needed to ensure that the optimal process and control design remains feasible and stable in the presence of bounded disturbances. In the first stage, a simultaneous dynamic flexibility and feasibility analysis is performed to identify an optimal process and control design alternative that remains feasible in the presence of critical realizations in the disturbances. A robust stability test is performed in the second stage to evaluate the asymptotic stability of the system obtained from the first stage.

As show in Figure 3, a set $\mathbf{Z}$ is introduced in the algorithm to store solutions obtained from the dynamic flexibility and feasibility formulation that did not satisfy the robust stability test (see the stability test section). This set $\mathbf{Z}$ is defined as follows

$$\begin{aligned} \mathbf{Z} &= \{\mathbf{Z}(1), ..., \mathbf{Z}(j)\} \\ \mathbf{Z}(j) &= \{\boldsymbol{\psi}_Z(j), \boldsymbol{\omega}_Z(j), \boldsymbol{\eta}_Z(j), \mathbf{y}_Z(j), \boldsymbol{\lambda}_Z(j)\} \end{aligned} \tag{7}$$

where $\mathbf{Z}(j)$ represents the solution set obtained from the dynamic flexibility and feasibility analysis at the j^{th} iteration step (see Figure 3) and that have not complied with the robust stability test. The formulation shown in (8) is included in the dynamic flexibility and feasibility formulation to avoid the reselection of solution sets that were identified as unstable by the robust stability test. Ξ_i is a smooth approximation function used to exclude from the dynamic flexibility and feasibility analysis those process and control designs that have been identified as unstable. The inequality constraints shown in (8) on $\boldsymbol{\eta}$, $\mathbf{y}$ and $\boldsymbol{\lambda}$ become active when a process design alternative ($\boldsymbol{\psi}$) and a multiloop control scheme ($\boldsymbol{\omega}$) selected in the dynamic flexibility and feasibility analysis are the same to that included in any of the solution sets in $\mathbf{Z}$. M_L is a sufficiently large number. The tolerance criterion parameters ε_η, ε_y, and ε_λ specify how far or how close the

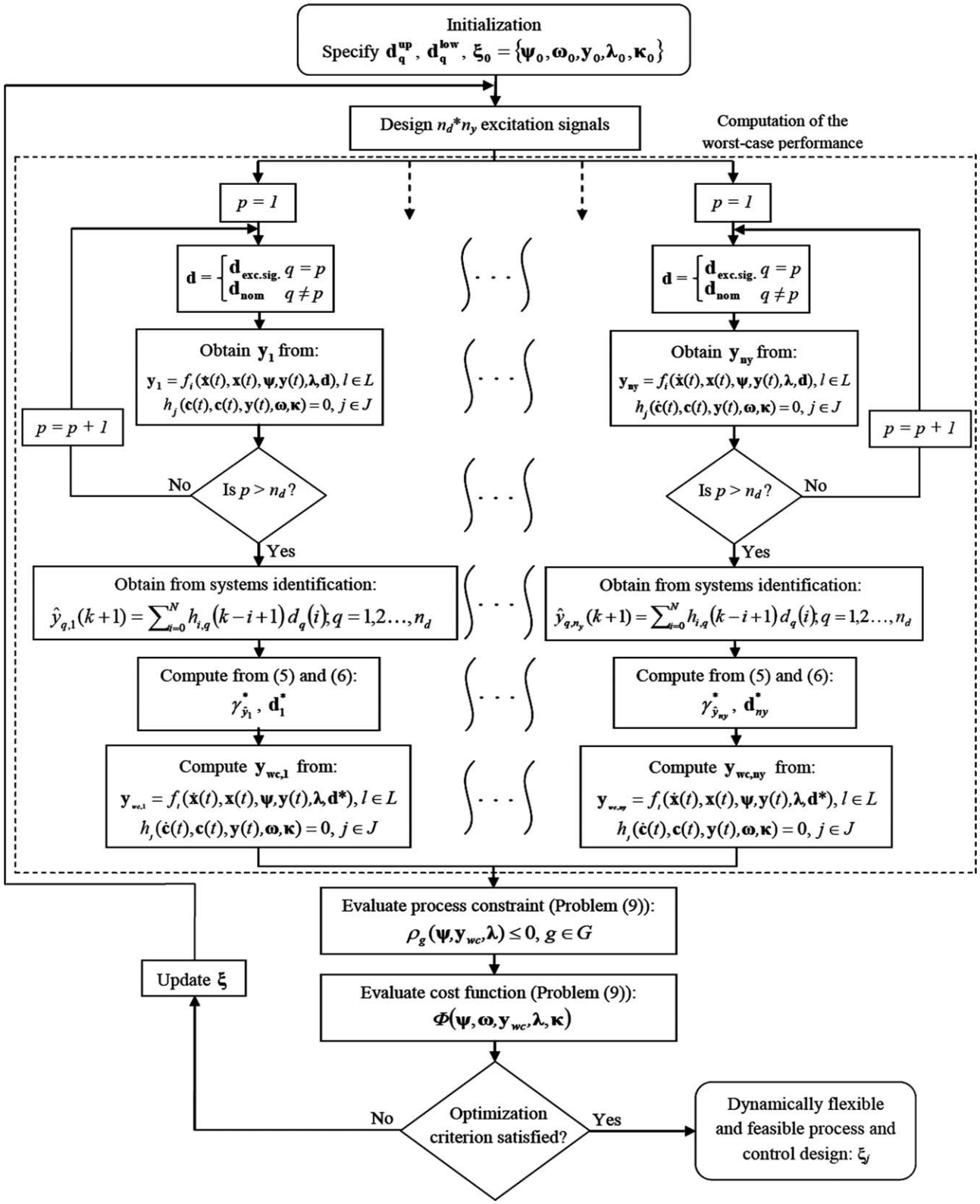

Figure 2. Algorithm for the simultaneous evaluation of dynamic flexibility and dynamic feasibility.

dynamic flexibility and feasibility formulation is allowed to select values for $\boldsymbol{\eta}$, $\mathbf{y}$ and $\boldsymbol{\lambda}$ for process flow sheets and control structures included in $\mathbf{Z}$. Estimates for these parameters depend on the desired accuracy in the solution and the computational infrastructure available. Setting ε_η, ε_y, and ε_λ between 0.05–0.1 seem appropriate for this analysis. For example, if the dynamic flexibility and feasibility analysis selects a values in $\boldsymbol{\psi}$ and $\boldsymbol{\omega}$ that are the same as in $\mathbf{Z}(i)$, i.e.,$\boldsymbol{\psi}_Z(i), \boldsymbol{\omega}_Z(i)$ then the constraints on $\boldsymbol{\eta}$, $\mathbf{y}$ and $\boldsymbol{\lambda}$ in (8) are active and ensure that the solution obtained for $\boldsymbol{\eta}$, $\mathbf{y}$ and $\boldsymbol{\lambda}$ by the dynamic flexibility and feasibility analysis is at least 5–10% different from that included in $\mathbf{Z}(i)$

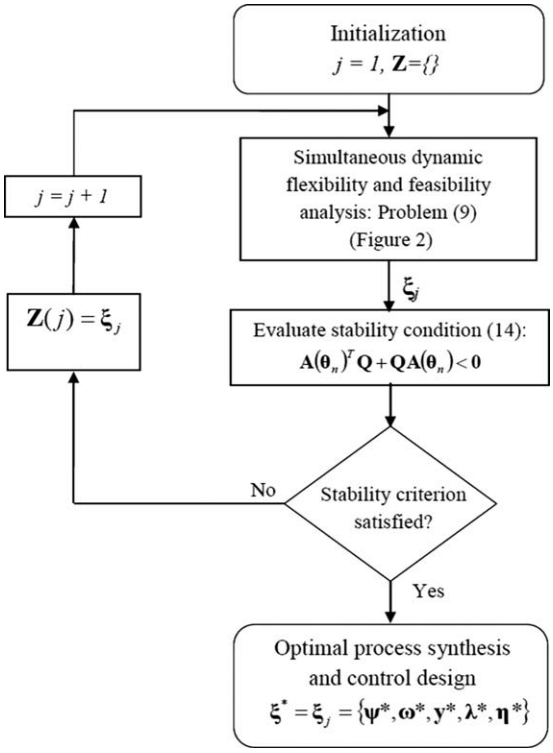

Figure 3. Simultaneous process synthesis and control design algorithm.

$$
\begin{aligned}
&(1-\Xi_i)\left(\left|\frac{\eta-\eta_Z(i)}{\max(\eta,\eta_Z(i))}\right|-\varepsilon_\eta\right)\geq 0 \qquad \forall i=1,\ldots,j\\
&(1-\Xi_i)\left(\left|\frac{y-y_Z(i)}{\max(y,y_Z(i))}\right|-\varepsilon_y\right)\geq 0 \qquad \forall i=1,\ldots,j\\
&(1-\Xi_i)\left(\left|\frac{\lambda-\lambda_Z(i)}{\max(\lambda,\lambda_Z(i))}\right|-\varepsilon_\lambda\right)\geq 0 \qquad \forall i=1,\ldots,j\\
&\boldsymbol{\Xi}=\{\Xi_1,\ldots,\Xi_i,\ldots,\Xi_j\}\\
&\Xi_i=\tanh\left\{M_L\left(\sum_{\psi}(\psi-\psi_Z(i))^2+\sum_{\omega}(\omega-\omega_Z(i))^2\right)\right\}
\end{aligned}
\tag{8}
$$

Problem (9) presents the formulation proposed here to perform the simultaneous dynamic flexibility and feasibility analysis in the presence of critical realizations in the disturbances. The optimization variables include the set of nonnegative integer decision variables ($\boldsymbol{\psi}$), which specify the process flow sheet superstructure; the set of binary decision variables ($\boldsymbol{\omega}$), which includes the different control configurations considered in the analysis (control superstructure); the set of continuous process design variables ($\boldsymbol{\eta}$) that specify the sizes of the units included in the process flow sheet specified by $\boldsymbol{\psi}$; the set of continuous process variables that determine the operating state of the system ($\mathbf{y}$); and the set of the controller tuning parameters ($\boldsymbol{\lambda}$). The set $\mathbf{y}$ may include the process set points, i.e., $\mathbf{v}$ in problem (4), and the nominal values in the variables that can be adjusted to control the operation of the system, i.e., $\mathbf{u}$ in problem (4). The set of decision variables in (9) define the system's nominal operating state $\boldsymbol{\xi}$. Following (9), $\mathbf{y_{wc}}\in\Re^{n_y}$ represents the worst-case performance of those process outputs that are included in the process constraints $\boldsymbol{\rho}$ and the cost function Φ. The elements in $\mathbf{y_{wc}}$ are obtained from simulations of the complete closed-loop process model in closed-loop (f and h). The inputs to those simulations are the critical realization in the disturbances, e.g., $\mathbf{d_p^*}$, which produce the worst-case performance in a process output, e.g., $\hat{\mathbf{y}}_\mathbf{p}$. To obtain $\mathbf{d_p^*}$, the identification of an uncertain model such as (3) and the search of $\gamma^*_{\hat{y}_p}$ from the roots problem posed in (5) is required. Logical constraints on the set $\boldsymbol{\omega}$ have been included in (9) to ensure that the multiloop control configuration selected by the optimization algorithm is feasible. Also, problem (9) includes the formulation (8) to ensure that previous solutions that did not comply with the stability test cannot be-reselected as optimal designs

$$
\begin{aligned}
&\min_{\xi=\{\psi,\omega,y,\lambda,\eta\}}\ \Phi(\boldsymbol{\psi},\boldsymbol{\omega},\mathbf{y_{wc}},\boldsymbol{\eta},\boldsymbol{\lambda})\\
&s.t.\\
&\quad f_l(\dot{\mathbf{x}}(t),\mathbf{x}(t),\boldsymbol{\psi},\mathbf{y}(t),\boldsymbol{\eta},\mathbf{d}),l\in L\\
&\quad h_j(\dot{\mathbf{c}}(t),\mathbf{c}(t),\mathbf{y}(t),\boldsymbol{\omega},\boldsymbol{\lambda})=0,j\in J\\
&\quad \rho_g(\boldsymbol{\psi},\mathbf{y_{wc}},\boldsymbol{\eta})\leq 0,g\in G\\
&\quad \sum_{n=1}^{N}\omega_{n,m}\leq 1\\
&\quad \sum_{m=1}^{M}\omega_{n,m}\leq 1\\
&\quad \boldsymbol{\omega}=[\omega_{1,1},\ldots,\omega_{n,m},\ldots,\omega_{N,M}]\\
&\quad \omega_{n,m}=\{0,1\}\\
&\quad \mathbf{d}^*=\{\mathbf{d_1^*},\ldots\mathbf{d_q^*},\ldots\mathbf{d_{n_d}^*}\}\\
&\quad \mathbf{y_{wc}}=[y_{wc,1},\ldots,y_{wc,p},\ldots,y_{wc,ny}]\\
&\quad \text{constraints}\quad (8)\\
&\quad \mathbf{y}=\{y,y_l\leq y\leq y_u\}\\
&\quad \boldsymbol{\lambda}=\{\lambda,\lambda_l\leq\lambda\leq\lambda_u\}\\
&\quad \boldsymbol{\eta}=\{\eta,\eta_l\leq\eta\leq\eta_u\}\\
&\quad \boldsymbol{\psi}\in Z^+
\end{aligned}
\tag{9}
$$

As shown in (9), ρ_g represents the constraints that ensure the feasible operation of the system. The worst-case performance tool can be employed to evaluate dynamic path constraints due to critical realizations in the disturbances. For example, the following constraint represents a purity constraint in one of the distillates in a distillation column (see case study 2 section)

$$
x_{dist}^{\text{target}}-x_{dist}(t)\leq 0\Longleftrightarrow x_{dist}^{\text{target}}-x_{dist,wc}^{\max}\leq 0 \tag{10}
$$

where x_{dist}^{target} is a user-defined concentration target for a distillate, whereas $x_{dist}(t)$ represents the composition of that distillate at any time t and that is calculated from the process model equations f_l. Thus, an UFIR model such as (3) that captures the key process dynamics between the disturbances $\mathbf{d}$, e.g., random changes in the feed-stream composition, and $x_{dist}(t)$ needs to be identified. Recall that the UFIR model captures the nonlinear behavior in $x_{dist}(t)$ due to changes in $\mathbf{d}$ since each of the UFIR model coefficients are defined as uncertain model parameters bounded by specific limits (see definition (3)). Hence, the nonlinearities between $x_{dist}(t)$ and $\mathbf{d}$ are explicitly accounted for in the evaluation of that nonlinear constraint since the uncertain model, which is used to obtain $x_{i,wc}^{\max}$, captures the process nonlinearities between these variables with the uncertain impulse response coefficients, i.e., $\delta h_{i,q}(k\text{-}i+1)$ in (3). As shown in the worst-case performance tool section, the μ-analysis problem shown in (5) needs to be solved first to obtain a bound on the worst-case performance output for $x_{dist}(t)$ $\left(\gamma^*_{x_{dist}}\right)$, and the normalized time-discrete realizations in $\mathbf{d}$ that produces such condition, i.e., Δ_d^* (see (A.6) in the supplementary material). The key entries to solve (5) are the UFIR model parameters,

i.e., $\bar{h}_{i,q}(k\text{-}i+1)$ and $\delta h_{i,q}(k\text{-}i+1)$, and the maximal deviations expected for the disturbances, δd (see definition (2)). Both $\gamma^*_{x_{dist}}$ and $\mathbf{\Delta}^*_d$ are used to calculate $\mathbf{d}^*_{x_{dist}}$ using (6). The critical time-discrete vector is then used as input to simulate the complete process model and controller equations using f_l and h_j, respectively. The largest (worst-case) variability in the positive direction for $x_{dist}\left(x^{\max}_{dist,wc}\right)$ can be extracted from the results of that simulation. The estimate for $x^{\max}_{dist,wc}$ is then used to evaluate the purity constraint on this variable as shown in (10). Although constraint (10) has an explicit linear form, it is a nonlinear dynamic path constraint since is a function of the process model (nonlinear) equations, e.g., $x_{dist}(t)$ behave in a nonlinear fashion due to changes in $\mathbf{d}$. As described in the worst-case performance tool section, the UFIR models are only valid around a nominal operating point defined by the optimization variables ($\boldsymbol{\xi}$) in the simultaneous process flow sheet and control design formulation shown in (9). Thus, UFIR models describing the dynamics between the process outputs (or constraints), and the disturbances need to be identified for each new set of values in $\boldsymbol{\xi}$ tested by the optimization algorithm used to solve (9). Accordingly, a robust performance analysis, which determines the worst-case performance in the outputs or constraints (ρ_g) due to critical realizations in the disturbances using UFIR models, is conducted at each optimization step via the solution of the structured singular value problem (5). The UFIR model parameters $\bar{h}_{i,q}(k-i+1)$ and $\delta h_{i,q}(k-i+1)$, are obtained from simulations of the actual nonlinear closed-loop process model following the systems identification procedure described in the worst-case performance tool section. Thus, the UFIR model coefficients are updated at every step in the optimization calculations, i.e., the quantification of uncertainty on each of the uncertain impulse response coefficients $\delta h_{i,q}(k-i+1)$, is recalculated at every optimization step. As shown in the computational performance section, this approach is more efficient than the direct computation of the worst-case performance from problem (4).

Dynamic path constraints can also be formulated as functions of multiple process outputs that may appear in a nonlinear form, e.g., a flooding restriction in a distillation column that needs to be satisfied at time t

$$D_{flood}(t)-D_{col}\leq 0 \tag{11}$$

where D_{col} is the distillation column's diameter; $D_{flood}(t)$ is the minimum column diameter required to avoid flooding in the column and which is defined as a nonlinear function of other time-varying outputs, e.g., the vapor flow rate, the flooding velocity and the liquid and vapor mass densities along the column. The nonlinear function, e.g., $D_{flood}(t)$, can be explicitly considered as a process output, and, thus, its worst-case performance calculated using the procedure described above for $x_{dist}(t)$. However, the UFIR model required to capture the process nonlinearities between D_{flood} and $\mathbf{d}$ may generate large values in $\delta h_{i,q}(k\text{-}i+1)$, which may subsequently produce large worst-case performance estimates for D_{flood}. An alternative approach consist in the independent evaluation of the worst-case performance of each of the outputs included in the nonlinear function, e.g., $D_{flood}(t)$. For example, the largest variability in the vapor flow rate along the column due to changes in the $\mathbf{d}$ is calculated using the method described in the section. The rest of the outputs required to evaluate the nonlinear function are obtained in the same fashion. The worst-case performances for the individual outputs are then used to evaluate the nonlinear function, e.g. $D_{flood}(t)$. Such evaluation returns an estimate on the variability expected for the nonlinear function due to changes in the disturbances. That is, this approach may not return the worst-case variability for the nonlinear function, e.g., $D_{flood}(t)$, since the function is evaluated using the individual worst-case performance outputs. Problem (9) can be solved using the two alternatives proposed here and select the design that suits the user's requirements.

The optimal process and control design formulation shown in (9) ensures that the entire operating range is dynamically feasible since it accommodates the worst-case deviations expected for the process operability constraints due to critical time-discrete realizations in the disturbances. On the other hand, the performance of the control system obtained by this method is expected to be conservative since the constraints are evaluated based on their worst-case deviations. The controllers' performance directly depends on the disturbance dynamics, which are assumed to be the only inputs affecting the system. Therefore, the major source of uncertainty in this analysis is the uncertainty in the time-discrete realizations in the disturbances, i.e., the disturbance dynamics, which generates the worst-case deviation in the constraints and in the process outputs. The structured singular value formulation shown in (5) aims to search, at every step in the optimization calculations, for the critical time-discrete disturbance profiles that generate such condition, i.e., the worst-case performance. The computation of the worst-case performance is then used to evaluate the compliance of the constraints and the cost function in simultaneous process flow sheet and control design formulation shown in (9).

As shown in the simultaneous design and control formulation (9), the control structure ($\boldsymbol{\omega}$) and their corresponding controllers' tuning parameters ($\boldsymbol{\lambda}$) are optimization variables that are selected such that they minimize the total plant costs and comply with the feasibility constraints in the presence of the critical time-discrete disturbance realizations that produce the worst-case deviations in the constraints. The worst-case deviations in the constraints are evaluated using the UFIR model, which represents the closed-loop dynamic behavior of the system and that is identified from simulations. Thus, the computation of the worst-case performance, and the corresponding evaluation of the constraints in problem (9), takes into account the selection made by the optimization algorithm used to solve (9) in terms of the control structure ($\boldsymbol{\omega}$) and their corresponding controllers' tuning parameters ($\boldsymbol{\lambda}$). Accordingly, the solution to problem (9) specifies a control structure and their corresponding controllers' tuning parameters that maintain the system within its feasible limits in the presence of the critical time-discrete realizations in the disturbances.

Problem (9) is an MINLP complemented with dynamic simulations of the complete closed-loop process model, i.e., f and h in problem (9). This formulation is different from previous dynamic optimization-based methodologies since they explicitly include as constraints the process model and control equations, which are usually discretized using finite element analysis or finite differences.[12–16,37] In this formulation, the process model equations are implicitly included as constraints and satisfied at the optimal solution since they are used for the computation of the worst-case performance in the process outputs, which are also satisfied at the optimal

solution. Also, this formulation estimates the critical disturbance set $\mathbf{d}^*$ using a norm-bounded technique (μ-analysis), which is a convex problem[50] that is more computationally efficient than the solution of a formal nonlinear optimization problem (see computational performance section). This is a new feature introduced by this algorithm since it enables the simultaneous evaluation of dynamic flexibility and feasibility, i.e., evaluate the dynamic flexibility of a given process flow sheet and control structure alternative by testing the dynamic feasibility of that alternative using the critical realizations in $\mathbf{d}$ that produces the largest (worst-case) performance for the process outputs. To the authors' knowledge, problem (9) is the first formulation proposed to perform both dynamic flexibility and feasibility simultaneously for optimal process synthesis and control structure design.

Stability test

Problem (9) returns an optimal process flow sheet and control structure configuration that is feasible in the presence of the most critical time-discrete realizations in the disturbances, i.e., $\mathbf{d}^*$. To ensure the asymptotic stability of the process and control design obtained from (9), this methodology incorporates a robust stability test in the algorithm as shown in Figure 3. In order to obtain estimates for the system states, the dynamic behavior of the complete closed-loop process model needs to be represented as a state space model, i.e.

$$\begin{aligned} \dot{\mathbf{x}} &= \mathbf{A}x + \mathbf{B}\hat{\mathbf{d}}_{\mathbf{q}} \\ \hat{\mathbf{y}}_{\mathbf{p}} &= \mathbf{C}x \end{aligned} \tag{12}$$

where $\hat{\mathbf{d}}_{\mathbf{q}}$ represents the effect of the q^{th} disturbance (in deviation form) to the p^{th} output. The elements of matrices $\mathbf{B}$ and $\mathbf{C}$ are assumed to be real scalars, whereas each of the elements in the $\mathbf{A}$ state-space matrix $(a_{i,j})$ is assumed to be given by a range of values defined as follows

$$\mathbf{A} = \left\{ a_{i,j} | a_{i,j} \leq \bar{a}_{i,j} \pm \delta a_{i,j} \right\} \tag{13}$$

where $\bar{a}_{i,j}$ is the nominal value in the i,j element of the $\mathbf{A}$ state-space matrix, whereas $\delta a_{i,j}$ represents the uncertainty associated with that element in the matrix $\mathbf{A}$. As in the UFIR model (3), the $\delta a_{i,j}$ are used to capture the nonlinearities in the system states due to changes in the disturbances $\mathbf{d}$. State-space models with an uncertain matrix $\mathbf{A}$ can be also be identified using the procedure described in the section.

The robust stability test proposed in this work is based on the concept of Lyapunov theory[51–53] and is as follows (the complete derivation of the robust stability test is shown in the supplementary material, Section C)

$$\begin{aligned} &\mathbf{A}(\theta_\iota)^T\mathbf{Q} + \mathbf{Q}A(\theta_\iota) < \mathbf{0} \\ &\theta = \{\theta_1, \ldots, \theta_\iota, \ldots, \theta_{2^\iota}\} \\ &\theta_\iota \in \left\{ \bar{a}_{i,j} - \delta a_{i,j}, \bar{a}_{i,j} + \delta a_{i,j} \right\} \\ &\mathbf{Q} = \mathbf{Q}^T, \mathbf{Q} > \mathbf{0} \end{aligned} \tag{14}$$

where $\boldsymbol{\theta}$ denotes the set of 2^ι vertexes specified by the different combinations between the extreme values of each of the $a(i,j)$ elements in matrix $\mathbf{A}$. $\mathbf{Q}$ is a positive definitive matrix that is independent of the system states and is also known as the *Lyapunov matrix*. The inequality constraint in (14) is a finite set of linear matrix inequalities (LMI's), each evaluated at the vertexes included in the set $\boldsymbol{\theta}$. The robust stability test states that the system, with states are given by the uncertain matrix $\mathbf{A}$, is asymptotically stable if there exists a positive definitive matrix $\mathbf{Q}$ that satisfies the LMI's shown in (14). The uncertain parameters of the state-space model shown in (12), i.e., $\delta a_{i,j}$ in (13), are the key inputs to evaluate the process asymptotic stability in the presence of magnitude-bounded disturbances using the robust stability test (14). The uncertain terms $\delta a_{i,j}$ are used to capture the system's nonlinearities due to changes in the disturbances and do not represent the uncertainty in one (or a few) of the parameters of the actual process model equations. As in the worst-case performance tool, the only inputs considered to evaluate the closed-loop stability are the disturbances. Thus, the major source of uncertainty in the stability test is also the uncertainty associated with the time-discrete realizations in the disturbances that may generate process instability. Accordingly, a robust stability analysis using (14) is performed on every optimal process flow sheet and control design configuration obtained from problem (9) to ensure that the system is asymptotically stable in the presence of disturbances. Numerical subroutines that can efficiently evaluate LMIs similar to that shown in (14) are available, e.g., the LMI toolbox in MATLAB®.[54] Although condition (14) may be added as a constraint in problem (9), this solution strategy may only work for systems with a small number of process units[22,27] since the stability test is computationally intensive for large-scale systems. To reduce the computational costs, this method only implements the robust stability test (14) on the solutions obtained from the dynamic flexibility and feasibility formulation, i.e., the stability test is performed outside problem (9). This new approach introduced by this algorithm (see Figure 3) ensures that the solution obtained from (9) is asymptotically stable without the need to sacrifice computational speed. Process stability is key in optimal process design. Previous designs obtained by simultaneous design and control methodologies that did not include a stability test have been found to be unstable.[44] In addition, only a few methods have included a formal stability analysis in their formulation.[16,37,44]

Following Figure 3, if the solution obtained from (9) at the j^{th} iteration (ξ_j) does not comply with condition (14), then update (augment) the set $\mathbf{Z}$ shown in (7) with the set as follows

$$\mathbf{Z}(j) = \xi_j = \left\{ \boldsymbol{\psi}_Z(j), \boldsymbol{\omega}_Z(j), \boldsymbol{\eta}_Z(j), \mathbf{y}_Z(j), \boldsymbol{\lambda}_Z(j) \right\} \tag{15}$$

The new (augmented) set $\mathbf{Z}$ is the key input to perform the dynamic flexibility and feasibility analysis at the next iteration, i.e., $j = j + 1$. The set $\mathbf{Z}$, embedded in (9) through the formulation shown in (8), ensure that the previous process and control design configurations, which were identified as unstable, cannot be reselected as optimal from problem (9). On the other hand, if condition (14) is satisfied for the current set ξ_j, then STOP, an optimal process synthesis and control structure design that remains feasible and asymptotically stable in the presence of critical realizations in the disturbances have been identified, i.e., $\xi^* = \xi_j$.

Case Study 1: A System of CSTR's connected in Series

The methodology presented in the previous section was applied for the optimal process and control design of a system of continuous stirred-tank reactors (CSTRs) connected series. As shown in Figure 4, the process flow sheet superstructure for this case study considers two CTSRs connected in series and a maximum of two inlet feed streams. An

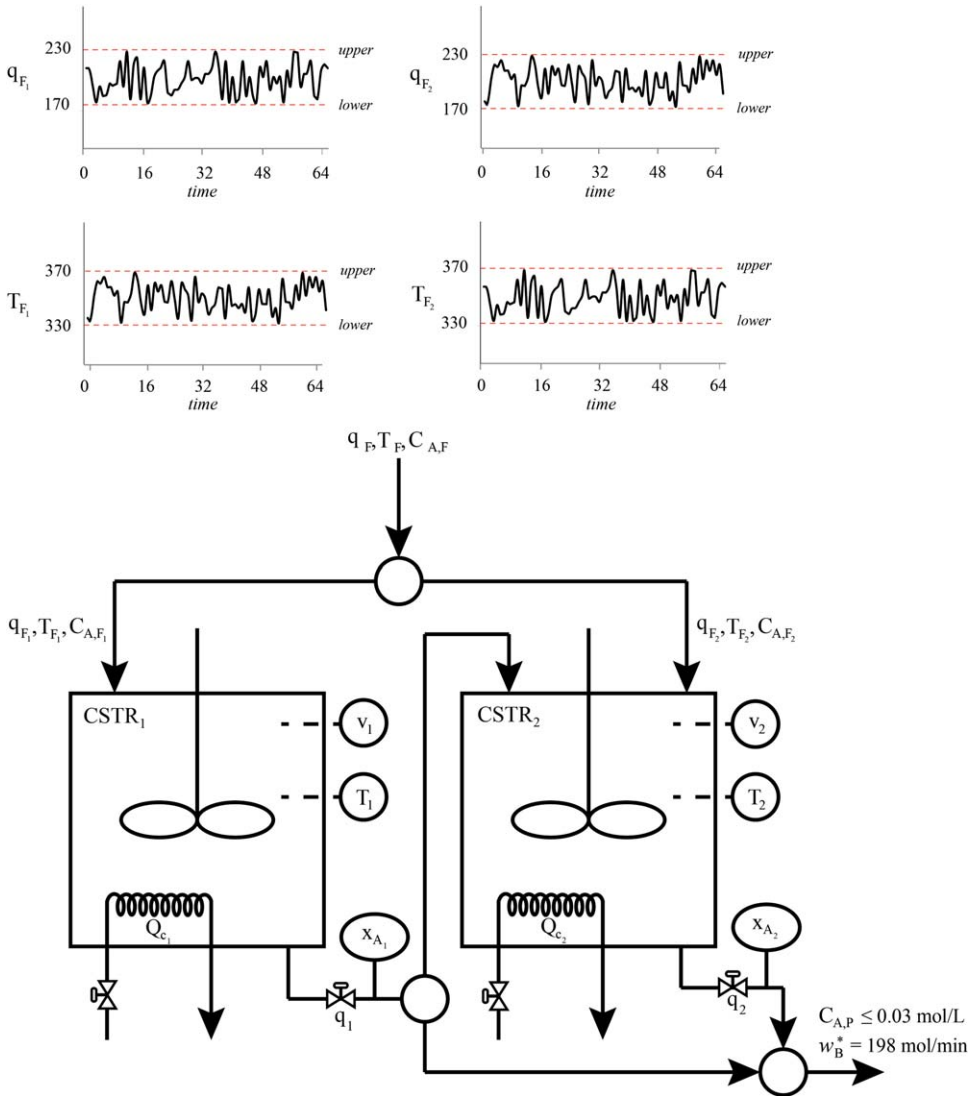

Figure 4. Process flow sheet superstructure: System of CSTRs in series.

[Color figure can be viewed in the online issue, which is available at wileyonlinelibrary.com].

exothermic irreversible reaction that transforms reactant A into product B is assumed to occur on both reactors, i.e., $A \rightarrow B$. The mechanistic model for this system is shown in (16). The binary variable D determines the existence of the second CSTR, whereas the binary variable R determines the existence of a second inlet feed stream that enters the second CSTR, i.e., the set $\boldsymbol{\psi}$ in (9) is defined for this case study as $\boldsymbol{\psi}=\{D,R\}$. Hence, this case study considers three process synthesis decisions: (1) a single reactor with one inlet feedstream ($D=R=0$), (2) two reactors with a single feed stream entering the first reactor ($D=1$, $R=0$), and (3) two reactors with two feedstreams, each feedstream entering each reactor ($D=R=1$). As shown in (16), the states of the system are specified by the liquid level, the temperature and the concentration of reactant A inside each reactor. Following (16), s ($0<s<1$) denotes the feed flow rate for the first and the second feedstream, respectively, E represents the activation energy (83,145 J/mol), k_0 is the pre-exponential factor (7.2e-10), R is the gas universal constant (8.3144 J/mol-K), C_p represents the liquid's heat capacity (0.239 J/g-K), ΔH_0 is the heat of reaction (4.78e4 J/mol), ϑ is the density of the fluid (1e3 kg/m^3). Furthermore, $C_{A,F1}$ (1 mol/L) and $C_{A,F2}$ (1 mol/L) represent the concentration of reactant A in the inlet streams

$$
\begin{aligned}
&\dot{V}_1 = q_{F1} - q_1 \\
&\dot{T}_1 = \frac{q_{F1}(T_{F1}-T_1)}{V_1} + \frac{\Delta H k_0 C_{A,1} \exp\left(\frac{-E}{RT_1}\right)}{\vartheta C_p} - Q_{c1} \\
&\dot{C}_{A,1} = \frac{q_{F1}\left(C_{A,F1}-C_{A,1}\right)}{V_1} - k_0 C_{A,1} \exp\left(\frac{-E}{RT_1}\right) \\
&\dot{V}_2 = D(q_{F2}+q_1-q_2) \\
&\dot{T}_2 = D\left(\frac{q_{F2}(T_{F2}-T_2)}{V_2} + \frac{q_1(T_1-T_2)}{V_2} + \frac{\Delta H k_0 C_{A,2} \exp\left(-\frac{E}{RT_2}\right)}{\vartheta C_p} - Q_{c2}\right) \\
&\dot{C}_{A,2} = D\left(\frac{q_{F2}\left(C_{A,F2}-C_{A,2}\right)}{V_2} + \frac{q_1\left(C_{A,1}-C_{A,2}\right)}{V_2} - -k_0 C_{A,2} \exp\left(\frac{-E}{RT_2}\right)\right) \\
&Q_{c1} = 48.1909\kappa_1 \\
&q_1 = 10\kappa_2\sqrt{V_1} \\
&Q_{c2} = 48.1909 D\kappa_3 \\
&q_2 = 10D\kappa_4\sqrt{V_2} \\
&q_{F1} = q_F(1-sRD) \\
&q_{F2} = q_F sRD
\end{aligned}
\tag{16}
$$

Table 1. Optimal Process and Control Design Structure: System of CSTRs in Series

	Optimal design: OD	One CSTR, one inlet stream: (PF1)	Two CSTRs, one inlet stream: (PF2)
Process flowsheet	D=1, R=1, s=0.52	D=0, R=0, s=0 (fixed)	D=1, R=0, s=0 (fixed)
Control Structure	ζ_1-T_1: K_C=-50.015, τ_I=50	ζ_1-T_1: K_C=-10, τ_I=48.03	ζ_1-T_1: K_C=-9.60, τ_I=20.38
	ζ_2-V_1: K_C=-0.1, τ_I=0.89	ζ_2-V_1: K_C=-0.088, τ_I=0.0153	ζ_2-V_1: K_C=-0.1, τ_I=0.0001
	ζ_3-C_{A2}: K_C=13.33, τ_I=0.34		ζ_3-C_{A2}: K_C=13.36, τ_I=0.50
	ζ_4-V_2: K_C=-0.1, τ_I=0.97		ζ_4-V_2: K_C=-0.001, τ_I=0.274
Operating conditions	T_1^*=470 K	T_1^*=499 K	T_1^*=499 K
	$C_{A,2}^*$=0.01 mol/L	$C_{A,1}^*$=0.01 mol/L	$C_{A,2}^*$=0.01 mol/L
	V_1^*=45.89 L	V_1^*=134 L	V_1^*=39.59 L
	V_2^*=138.34 L		V_2^*=3.51 L
Annualized Costs			
CC ($/yr)	1,797.60	1,450.09	728.72
DPC ($/yr)	9,595.65	15,481.52	15,622.98
Φ_{CSTR} ($/yr)	11,393.24	16,932.43	16,351.71

The control scheme considered for this case study is a multiloop feedback control strategy composed of proportional-integral (PI) controllers. As shown in Figure 4, the manipulated variables for this process are the flow rates at the outlet of each CSTR (q_1 and q_2) and the cooling heat flow on each reactor, (Q_{c1} and Q_{c2}). The variables κ_i in (16) are the control inputs for each manipulated variable. Likewise, the temperature, the liquid level, and the concentration of reactant A on each reactor, i.e., T_1, V_1, $C_{A,1}$, T_2, V_2, $C_{A,2}$, are the controlled variables. The set of multiloop control schemes considered for this process is as follows

$$\begin{aligned}
&\dot{c}_{nm}=\omega_{nm}\left(\frac{e_{nm}}{\tau_{Inm}}\right)\\
&\kappa_n=\bar{\kappa}_n+\sum_{m=1}^{6}\Delta\kappa_{nm}\\
&\Delta\kappa_{nm}=\omega_{nm}K_{Cnm}(e_{nm}+c_{nm})\\
&e_{nm}=z^*_{nm}-z_{nm}\\
&\sum_{n=1}^{2}\omega_{nm}\le 1 \qquad \forall m=1,2,3\\
&\sum_{n=3}^{4}D\omega_{nm}\le 1 \qquad \forall m=4,5,6\\
&\sum_{m=1}^{3}\omega_{nm}\le 1 \qquad \forall n=1,2\\
&\sum_{m=4}^{6}D\omega_{nm}\le 1 \qquad \forall n=3,4\\
&\omega_{nm}=\{0,1\}
\end{aligned} \tag{17}$$

where the binary variables ω_{nm}'s specify a particular multiloop control structure (see problem (9)). The inequality constraints shown in (17) are the logical constraints shown in (9) that ensure that only one manipulated variable can be paired with one controlled variable in a control loop, i.e., it guarantees the feasibility of the multiloop control structure selected by the optimization algorithm. Following (17), the subscripts n and m represent the manipulated and the controlled variables for this case study, respectively. To simplify the analysis, this control superstructure only includes control loops between manipulated variables and controlled variables located on the same process unit. Thus, m = 1,2,3 (T_1, V_1, $C_{A,1}$) and n = 1,2 (q_1, Q_{c1}) represent the controlled variables and the manipulated variables for the first CSTR, whereas m = 4,5,6 (T_2, V_2, $C_{A,2}$) and n = 3,4 (q_2, Q_{c2}) are the controlled variables and manipulated variables for the second CSTR, respectively. Hence, $\boldsymbol{\omega} = \{0,1\}^{nxm}$ contains 12 binary decision variables, whereas the sets $\mathbf{K_C} \in \Re^{nxm}$ and $\boldsymbol{\tau_I} \in \Re^{nxm}$, the PI tuning parameters, consider 12 continuous decision variables. $\bar{\kappa}_n$ is a nominal (steady-state) value in the control input κ_n, whereas $\Delta\kappa_{nm}$ denotes the control action. The flow rate and the temperature of each of the inlet feedstreams included in the process flow sheet superstructure (q_{F1}, T_{F1}, q_{F2} and T_{F2}) are assumed to be unmeasured variables that are subject to random fluctuations due to changes in the upstream process. Thus, these inputs represent the disturbances for this process and are defined as follows

$$\begin{aligned}
&\mathbf{d}=\{\mathbf{q_{F1}},\mathbf{T_{F1}},\mathbf{q_{F2}},\mathbf{T_{F2}}\}\\
&\mathbf{q_{F1}}=\{q_{F1}|q_{F1}=200(1-sRD)\pm 30(1-sRD)\} \qquad (L/\min)\\
&\mathbf{T_{F1}}=\{T_{F1}|T_{F1}=350\pm 20\} \qquad (K)\\
&\mathbf{q_{F2}}=\{q_{F2}|q_{F2}=200sRD\pm 30sRD\} \qquad (L/\min)\\
&\mathbf{T_{F2}}=\{T_{F2}|T_{F2}=350\pm 20\} \qquad (K)
\end{aligned} \tag{18}$$

The goal for this case study is to specify an optimal process synthesis and control design that continuously produces an outlet stream with a molar flow rate of product B of 198 mol/min. That is, the key design and control goal for this process is to obtain an outlet stream that maintains B's molar flow rate close to its target value in the presence of random fluctuations in the inlet feedstreams' flow rate and temperature. Also, the concentration of reactant A at the outlet (product) stream needs to be below 0.03 mol/L at all times. Moreover, the maximum and the minimum allowed operating temperature for each reactor is 500 K and 400 K, respectively. These temperature limits have to be satisfied at all times in the presence of fluctuations in the feedstreams' flow rate and temperature. Section C in the supplementary material shows the key steps to obtain the optimal process design for this case study using this simultaneous process synthesis and control design methodology.

Table 1 presents the results obtained for this case study. As shown in that table (optimal design, OD), the method specifies a process flow sheet that includes two CSTRs together with two inlet feedstreams. Likewise, the simultaneous optimal design and control formulation specified four control loops for this process; two PI controllers are used to maintain the liquid levels in the CSTRs, whereas the other two feedback loops maintain the reactors' temperature within their operability limits and the concentration of reactant A close to its set point value (0.01 mol/L), which was obtained from the solution specified by the decision variables set. Figure 5 shows the worst-case performance obtained for the process outputs at the optimal solution. As shown in Figure 5, the temperature inside each reactor complies with the

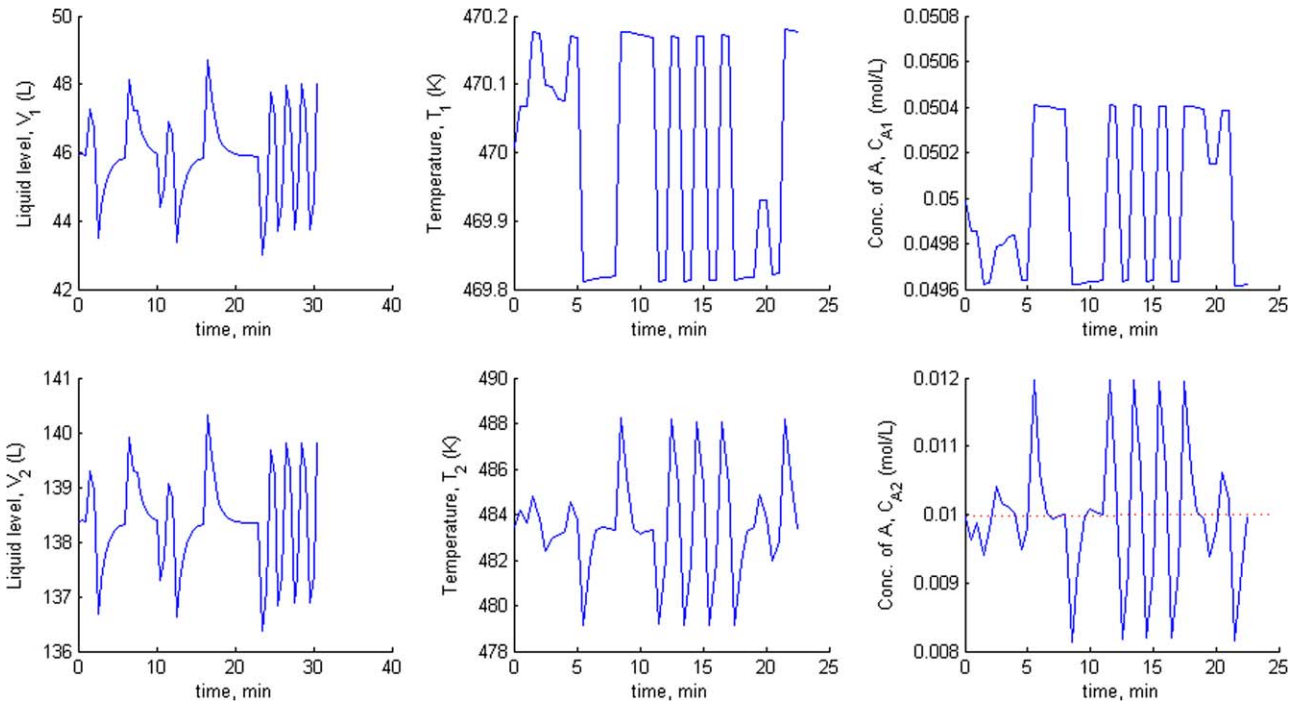

Figure 5. Worst case performance in the process outputs: System of CSTRs in series.

[Color figure can be viewed in the online issue, which is available at wileyonlinelibrary.com].

process feasibility constraints specified for this variable, whereas the concentration of reactant *A* at the product stream ($C_{A,2}$) oscillates closely to its set point value in the presence of critical realizations in the disturbances. Also, the liquid level on each CSTR fluctuates around their corresponding set point values (see Table 1). The stability of the process and control design specified by this method was verified by simulating the design using high- and low-frequency signals in the disturbances. No instabilities or constraint violations were observed from those simulations. Thus, the solution obtained by this method returned an optimal process synthesis and control design that is dynamically feasible and asymptotically stable in the presence of critical realizations in the disturbances.

In order to compare the results obtained by this method, this case study was relaxed and assumed that the process flow sheet remained fixed in the calculations. That is, the variables D and R, which determine the process flow sheet structure for this case study, were fixed in the analysis. Hence, the simultaneous design and control formulation seeks for the optimal control structure and operating conditions that complies with the process constraints at minimum annualized cost (Φ_{CSTR}). Hence, two additional optimal process and control designs were performed in this case study. The first scenario (PF1) involves a single CSTR with a single inlet feedstream ($D = 0$, $R = 0$, $s = 0$), whereas the second scenario (PF2) specified a process flow sheet with two CSTRs and one single feedstream ($D = 1$, $R = 0$, $s = 0$). The results obtained for each of these scenarios are presented in Table 1. As shown in Table 1, the optimal designs obtained for PF1 and PF2 are 32.71% and 30.32% more expensive than that obtained when process synthesis decisions were included in the simultaneous design and control formulation, respectively. Although the optimal design found by this method (OD in Table 1) specifies a capital cost that is 19.33% and 59.46% more expensive than that obtained for PF1 and PF2, the dynamic performance cost, which dominates the process economics, was reduced in OD by almost 38%with respect to PF1 and PF2, respectively. The significant savings in the case of the optimal process and control design (OD in Table 1) is mainly due to the selection of the process flow sheet structure, i.e., $D = 1$, $R = 1$. This process flow sheet allows a balanced distribution of the random fluctuations in the inlet feedstream flow rates between the two CSTRs, which reduce the variability in the liquid level, the temperature and the concentration of *A* in the reactors. This result is a clear indication that the process economics and the process' dynamic flexibility and dynamic feasibility are directly influenced by process synthesis and control structure decisions. Thus, process synthesis and control decisions are activities that need to be integrated in a single formulation for optimal process and control design, as it is considered in this methodology.

Case Study 2: A Ternary Distillation Column System

This section presents the application of the methodology proposed in this work for the simultaneous process synthesis and control design of a ternary distillation column, a typical chemical process widely used in the industry. This second case study is presented to demonstrate the effectiveness of this method to perform the optimal process and control design of challenging (complex) dynamic systems that are subject to critical realizations in the disturbances.

A graphical representation of the process superstructure considered for this case study is presented in Figure 6. The goal for this process is to separate a mixture of toluene, n-hexane and heptane into two streams with specific production targets. As shown in Figure 6, the distillation unit includes an overhead total condenser/reflux drum, a partial reboiler and a cooler located at the bottom of the unit. The

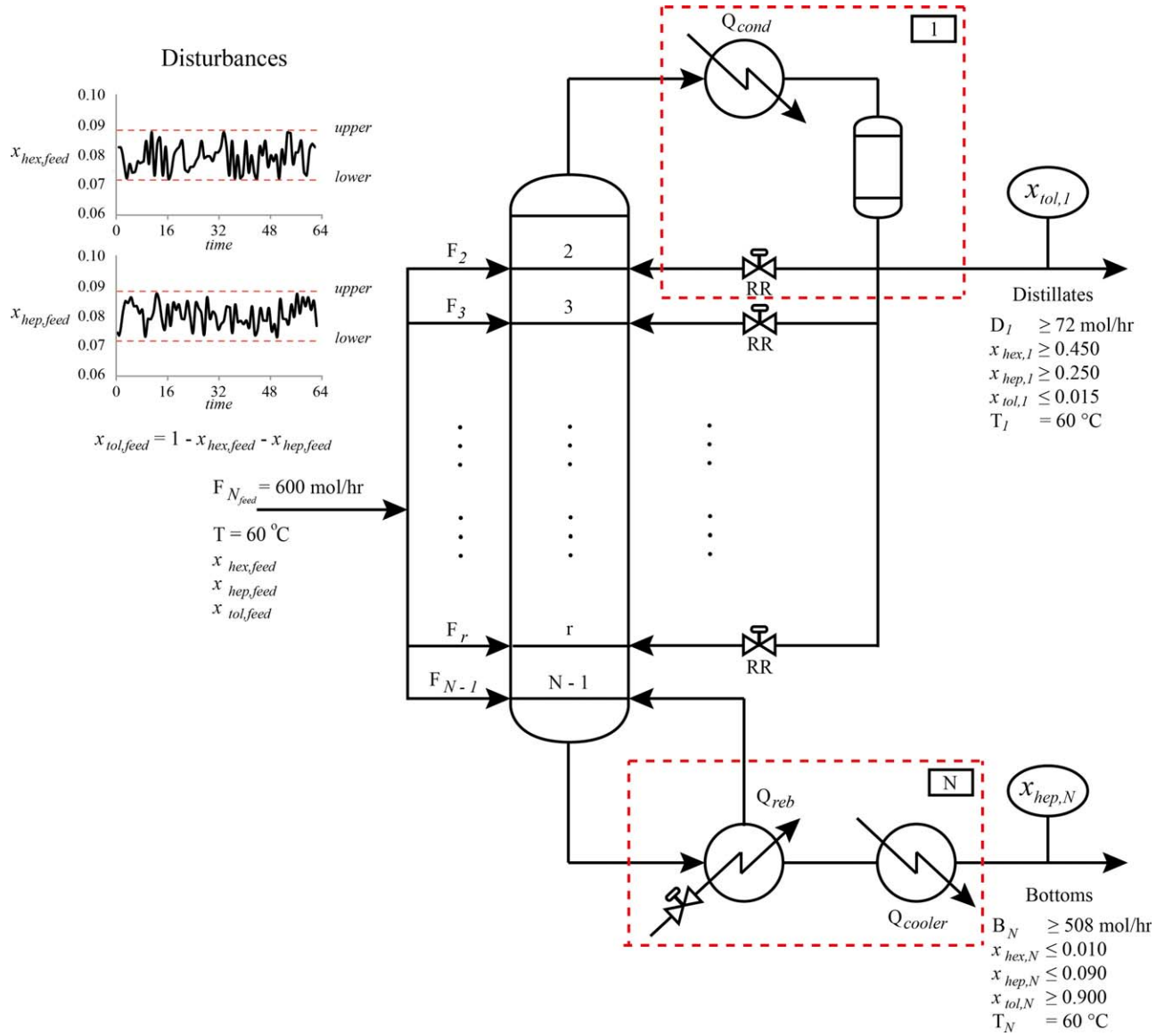

Figure 6. Process flow sheet superstructure: Ternary distillation unit.

[Color figure can be viewed in the online issue, which is available at wileyonlinelibrary.com].

distillation column considers N stages numbered from top to bottom, i.e., stage 1 represents the total condenser/reflux drum, whereas stage N represents the partial reboiler at the column base. The distillation column's feedstream contains a mixture of toluene, n-hexane and heptane and may enter the column at any stage between 1 and N. Following Figure 6, the reflux ratio (RR) and the heat duty in the reboiler unit (Q_{reb}) are considered to be adjustable variables that can be used to maintain the dynamic operability of this process within specs. Likewise, the system under consideration assumes that the composition of toluene at the top stream ($x_{tol,1}$) and the composition of heptane at the bottom stream ($x_{hep,N}$) are variables that can be measured online and are available for control. A multiloop control strategy composed of feedback controllers of type PI was considered in the formulation. A set of binary decision variables ($\boldsymbol{\omega}$) are included in the control superstructure formulation to specify the pairings (control loops) between the manipulated variables and the controlled variables considered for this system. Moreover, this analysis assumes that the total condenser located at the top of the column operates at a constant pressure (P_{cond}). Therefore, P_{cond} is considered as an optimization variable in the simultaneous dynamic flexibility and feasibility formulation. This case study considers that the composition of heptane and n-hexane in the feedstream, i.e., $x_{hep,feed}$ and $x_{hex,feed}$, are random perturbations that cannot be measured online. Hence, $x_{hep,feed}$ and $x_{hex,feed}$ represent the disturbances ($\mathbf{d}$) for this process. The feedstream operating conditions, including the disturbance descriptions specified for $x_{hep,feed}$ and $x_{hex,feed}$, are shown in Table 2.

The dynamic behavior of this process is represented by a rigorous tray-by-tray mechanistic model that was adapted from Mohideen et al.[12] The complete process model superstructure considered for this case study is given as supplementary material (Section D). The distillation column model describes the time-varying fluctuations of toluene, n-hexane and heptane inside the column due to changes in the composition of the feedstream. The distillation column model also includes tray-by-tray energy conservation balances that describe the temperature distribution along the column at

Table 2. Feedstream Data and Product Specifications: Ternary Distillation Unit

Modeling aspects	Process variables	
Feedstream Conditions	Temperature (T_{feed})=60 C	
	Flowrate (F_{feed})=600 mol/hr	
	$x_{hex,feed}(t)=0.08\pm\delta x_{hex,feed}$	
	$x_{hep,feed}(t)=0.12\pm\delta x_{hep,feed}$	
	$x_{tol,feed}(t)=1-x_{hex,feed}-x_{hep,feed}$	
	$\delta x_{hex,feed}=0.008$	
	$\delta x_{hep,feed}=0.012$	
Product specifications	Distillates	Bottoms
	$D_1(t)\geq$ 72 mol/hr	$B_N(t)\geq$ 508 mol/hr
	$x_{hex,1}(t)\geq 0.45$	$x_{hex,N}(t)\leq 0.01$
	$x_{hep,1}(t)\geq 0.25$	$x_{hep,N}(t)\leq 0.09$
	$x_{tol,1}(t)\leq 0.015$	$x_{tol,N}(t)\geq 0.90$

any time due to changes in the process operating conditions, e.g., changes in the reboiler heat duty due to sudden fluctuations in the feedstream's composition. The control superstructure, also presented in supplementary material (Section D), includes the two control schemes considered for this process and their corresponding controllers' tuning parameters, i.e., $\mathbf{K_C}\in\Re^{2x2}$ and $\boldsymbol{\tau_I}\in\Re^{2x2}$. The two set points considered in the control superstructure are the composition of toluene at the top stream and the composition of heptane at the bottom stream, i.e., $x^*_{tol,1}$ and $x^*_{hep,N}$. As shown in Table 2, the two outlet streams need to comply at any time with specific product targets.

The goal for this case study is to search for the optimal design and control structure that is able to maintain the dynamic operation of the ternary distillation column within limits, i.e., satisfy the outlet streams' specifications, in the presence of the most critical random fluctuations in the composition of n-hexane and heptane at the feedstream. The simultaneous design and control methodology presented in the mathematical framework section was implemented on this ternary separation system. The integer decision variables considered for this problem are the number of stages in the column (N), the feedstream stage (N_{feed}) and the binary set $\boldsymbol{\omega}$, which specifies the multiloop PI control scheme. Likewise, the continuous decision variables are the pressure of the condenser at the top of the column (P_{cond}), the set point for the composition of toluene in the distillate $\left(x^*_{tol,1}\right)$, the set point for the composition of heptane at the column base $\left(x^*_{hep,N}\right)$, and the PI's controller tuning parameters, i.e., $\mathbf{K_C}$ and $\boldsymbol{\tau_I}$. The cost function specified for this process (Φ_{dist}) is presented in Section D of the supplementary material. The function Φ_{dist} is defined in terms of the sizes of the process units involved in the analysis, i.e., the distillation column's diameter, the number of trays, and the heat-transfer areas of the reboiler, the cooler and the condenser units, and the costs due to the water and steam consumption in the cooler, the condenser and the reboiler units, respectively. To ensure that the optimal process and control design is dynamically feasible in the presence of disturbances, this analysis incorporated the product specifications at the outlet streams (see Table 2) as dynamic path constraints in the dynamic flexibility and feasibility formulation. These constraints are formulated as shown in the mathematical framework section. For example, the constraint shown in (19) is included in this case study's MINLP formulation to ensure that the composition of toluene in the distillates complies with the process specifications in the presence of critical realizations in the compositions of heptane and n-hexane in the feedstream, i.e., $x_{hep,feed}$ and $x_{hex,feed}$. The variable $x^{\max}_{tol_{1,wc}}$ in (19) represents the worst-case increase in the composition of toluene in the distillates due to critical realizations in $x_{hep,feed}$ and $x_{hex,feed}$, respectively. The evaluation of the worst-case performance of an output variable due to changes in the disturbances has been explicitly described for the first case study in Section C of the supplementary material. That same procedure is used in this case study to evaluate the compliance with the process constraints in the presence of critical realizations in $x_{hep,feed}$ and $x_{hex,feed}$, respectively

$$x_{tol}(t)-0.015\leq 0 \Longleftrightarrow x^{\max}_{tol_{1,wc}}-0.015\leq 0 \qquad (19)$$

The dynamic flexibility and feasibility (MINLP) formulation specified for the ternary distillation unit was implemented in MATLAB®. The built-in function *ode23s*[57] was used to integrate the model and control equations that specify the process superstructure whereas the built-in function *glcdirect* was used to solve the resulting MINLP problem.

Table 3 shows the optimal process and control design specified for this case study using the methodology presented in this work. As shown in Table 3, a column containing 28 theoretical trays is needed to operate the ternary distillation unit specified for this case study. The feedstream enters the column at stage 22, whereas the optimal condenser pressure is 0.9334 atm. The reflux ratio is used to maintain the composition of toluene at the top stream at its target value whereas the composition of heptane at column base is maintained at its set point adjusting the partial reboiler heat duty. Figure 7 shows the worst-case performance expected for the composition of toluene, n-hexane and heptane in the distillates. This figure shows that the optimal design specified by this method maintains the products' composition within their limits in the presence of the critical realizations in the disturbances. As shown in Figure 7, constraint (19) is active at the optimal solution. Similarly, Figure 8 shows that the constraints on the distillate and molar flow rates are also active at the optimal solution. These results indicate that the optimal design obtained by this method is dynamic feasible in the presence of the most critical realizations in $x_{hep,feed}$ and $x_{hex,feed}$, respectively. Extensive simulations of the optimal design were conducted to ensure that the resulting design is stable in the presence of magnitude-bounded perturbations.

Table 3. Optimal Process and Control Design Structure: Ternary Distillation Unit

	Specifications
Process design	$N=28$
	$N_{feed}=22$
	$D_{col}=0.722$ m
	$A_{cond}=0.1795$ m^2
	$A_{reb}=0.1014$ m^2
	$A_{cool}=0.0250$ m^2
Control Structure	$x_{tol,1}$-RR: K_C=-48.89, τ_I=0.615
	$x_{hep,N}$-Q_{reb}: K_C=-35.55, τ_I=0.725
Operating conditions	$P_{cond}=0.9334$ atm
	$x^*_{tol,1}=0.0069$
	$x^*_{hep,N}=0.0733$
Annualized Costs	
Capital Cost ($/yr)	33,581.17
Operating Cost ($/yr)	1,376.20
Φ_{dist} ($/yr)	34,957.37

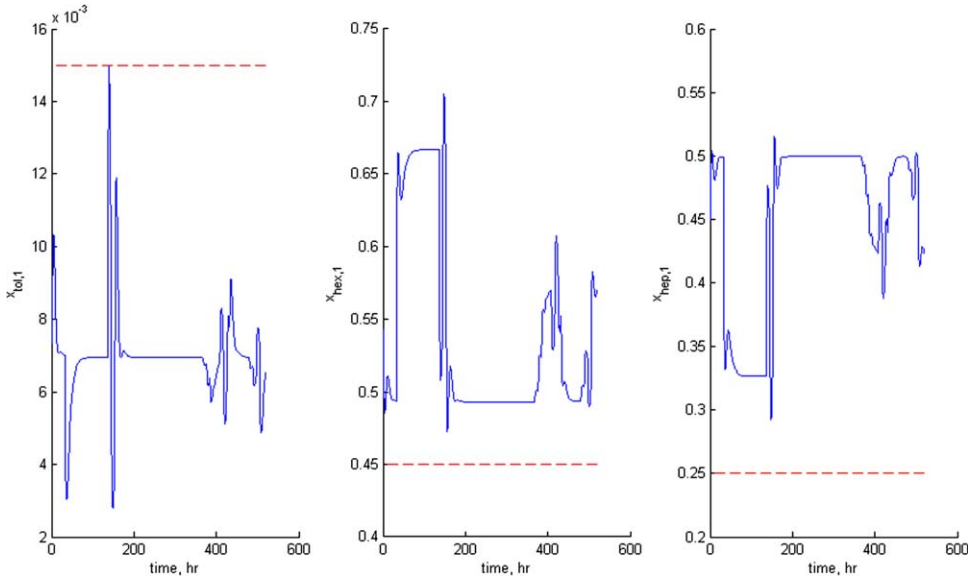

Figure 7. Worst case performance in the distillates' composition, Ternary distillation unit.

[Color figure can be viewed in the online issue, which is available at wileyonlinelibrary.com].

Therefore, the optimal design obtained for this case study is ensured to be dynamically feasible and asymptotically stable since it is able to accommodate the worst-case performance expected for the key process outputs and maintain the stable operation of the system under the influence of magnitude-bounded changes in the disturbances. The results presented in Table 3 also show that the capital cost dominates the process economics for this case study. Thus, this method aims to specify a system with the lowest number of trays and the smallest units' capacities that can comply with the process constraints and product specifications in the presence of critical realizations in the feedstream's composition.

This case study was also used by Mohideen and coworkers[12] to demonstrate the applicability of their simultaneous design and control methodology. Although the dynamic tray-by-tray process model used in this work is the same to that used by Mohideen,[12] a full comparison between the designs obtained by both methods is not possible due to the different assumptions made in solving this case study, e.g., the economic indicators in the cost function and the model coefficients in the dynamic model were taken from different sources. A qualitative comparison between the integration of process and control design approaches is described next.

While Mohideen at al.'s methodology required the sequential solution of two MINLPs to perform the dynamic flexibility and the dynamic feasibility analyses, this methodology performs both analyses simultaneously by solving a single MINLP complemented with dynamic simulations of the closed-loop process model. Although the closed-loop simulation of the process at each iteration step may increase the computational demands, this method enables the implementation of computer parallelization techniques, which reduces the computational effort in the calculations (see the computational performance section). Therefore, it is expected that this method is less computationally demanding than Mohideen et al.'s approach. Due to the use of gradient-based

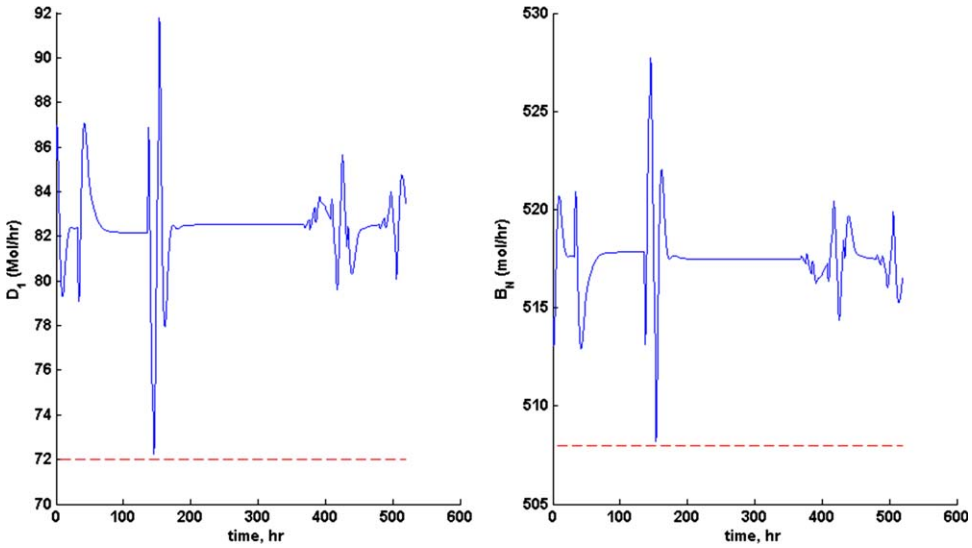

Figure 8. Worst case performance in the product streams' flow rates: Ternary distillation unit.

[Color figure can be viewed in the online issue, which is available at wileyonlinelibrary.com].

optimization methods, Mohideen's method required the specification of a time-dependent disturbance function with uncertain model parameters, e.g., a sinusoidal function with unknown amplitude and frequency. The goal in their dynamic feasibility analysis is to search for the critical values in the uncertain disturbance model parameters that generate constraint violations. Accordingly, the optimal design obtained by that method may not be valid for cases when the disturbance dynamics deviates significantly from the disturbance function used to attain the optimal process design. This method treats the disturbances as random time-discrete variables that can take any value that is bounded between upper and lower limits at a given time t. Hence, this methodology specifies a process design based on a more general disturbance description since it does not limit the disturbance dynamics to follow particular (user-defined) disturbance functions. On the other hand, Mohideen et al.'s methodology evaluates the dynamic feasibility test using the full nonlinear dynamic process model whereas this method evaluates such condition from the computation of the worst-case performance, which is based on the identification of a UFIR model that is only an approximation to the actual nonlinear closed-loop process model. Therefore, the direct calculation of the worst-case performance using the true process model may deviate from that obtained by this method. However, the rigorous computation of the worst-case performance using a general disturbance description is an intensive calculation that may become prohibitive for systems with a large number of states or process units.

Computational Performance

One of the key limitations in simultaneous design and control is the computational demands required to obtain the optimal design. The aim of this section is to present a study on the computational costs associated with this methodology. This analysis was performed on an Intel Core i7 CPU 930 @ 2.80 GHz (6.0 GB in RAM) with four physical cores.

The specification of the worst-case performance for a process output, i.e., the set $\mathbf{y_{wc}}$ in problem (9), represents the key calculation in this method since it needs to the performed as many times as process outputs and constraints are included in the dynamic flexibility and feasibility formulation. For example, case study 1 (system of CSTRs) requires the computation of the worst-case performance for six (four) process outputs when the binary decision variable D is set to be 1 (0). These computations must be redone for every new set of decision variables specified by the case study's MINLP optimization problem. Thus, the computation of a single worst-case performance can be used as a metric to estimate the computational costs of this approach. Hence, this analysis determined the CPU time required to evaluate the worst-case increase in the composition of toluene in the distillate $\left(x_{tol_{1,wc}}^{\max}\right)$, i.e., see constraint (19). The variable $x_{tol_{1,wc}}^{\max}$ was evaluated using the optimal solution obtained for the ternary separation system (see Table 3).

In order to evaluate the computational efficiency of this method, an alternative approach based on the computation of the worst-case performance using a formal dynamic optimization formulation was considered in this study. In principle, optimization problems similar to problem (4) need to be specified for every time-varying output that appears in the process constraints and in the cost function of the optimal design and control formulation. For example, $x_{tol_{1,wc}}^{\max}$ in (19) can also be obtained from the following optimization problem

$$\begin{aligned} &\max_{\mathbf{x}_{\mathbf{h}ep,feed},\mathbf{x}_{\mathbf{h}ex,feed}} \|x_{tol_1}\|_\infty \\ &s.t. \quad x_{tol_1} = f\left(\dot{\mathbf{x}}, \mathbf{x}, N, N_{feed}, x_{tol,1}^*, x_{hep,N}^*, \mathbf{x}_{\mathbf{h}ep,feed}, \mathbf{x}_{\mathbf{h}ex,feed}, P_{cond}, t\right) \\ &\quad h(\dot{\mathbf{c}}, \mathbf{c}, \boldsymbol{\omega}, \mathbf{K_C}, \boldsymbol{\tau_I}, t) = 0 \\ &\quad t = [0, t_f) \end{aligned} \tag{20}$$

where f and h represent the model and control equations of the process model superstructure specified for the ternary distillation unit, respectively. The solution to (20) returns the critical time-discrete vectors in $x_{hep,feed}$ and $x_{hex,feed}$ that produces the largest variability in x_{tol_1}, i.e., $x_{tol_{1,wc}}^{\max}$. Eq. 20 was solved in MATLAB® using *fmincon*, a built-in function that implements the sequential quadratic programming (SQP) algorithm.[58,59] The CPU time required for the evaluation of using both the method proposed in this work and dynamic optimization was recorded. The CPU time ratio between the approach presented in this work and the dynamic optimization scheme is 1:24 in favor of this method. That is, the computation of the worst-case performance using a dynamic optimization-based method is 24 times more intensive than the approach proposed in this work. Thus, the optimal design and control of complex systems like the ternary distillation unit using a formal dynamic optimization formulation for the computation of the worst-case performance results in higher computational costs than those required by this method. The worst-case performance approach proposed in this work is based on repeated systems identification and dynamic simulation of the process model for every new set of values in the design variables ($\boldsymbol{\xi}$) selected during the optimization calculations. Also, the dynamic optimization method used to solve problem (20) may not be the most efficient solution approach, i.e., sequential simulation and optimization. Thus, it is expected that the computational costs obtained by this study for the dynamic optimization problem may be improved when using other dynamic optimization techniques. Furthermore, the solution of these problems using other computational platforms, e.g., gPROMS, MUSCOD II, GAMS, may influence the outcome drawn from this comparison.

A key feature introduced by this approach is that the computation of the worst-case performance can be done independently, thus, allowing the implementation of computer parallelization techniques (see Figure 2). Therefore, significant savings in computational costs can be expected when the optimal process synthesis and control design method can be implemented using parallel programming. To test the computational benefits of this approach when using parallel programming, the codes used to obtain the optimal process synthesis and control design of the system of CSTRs and the ternary distillation unit were parallelized following the algorithm presented in Figure 2. The parallel codes were solved using *parfor*, a built-in function in MATLAB® that enables the use of multiple cores in parallel using multiple MATLAB workers.[60] Figure 9 shows the computational performance of this method when using multiple cores. As shown in (21), the computational performance specifies the reduction in computational time when the optimization function proposed by this approach is evaluated using multiple cores. As shown in Figure 9, the computational costs decreased by approximately 26% when four physical cores are used instead of a single core

$$\text{Computational performance} = 1 - \frac{\text{CPU time using } n \text{ cores}}{\text{CPU time using one core}} \tag{21}$$

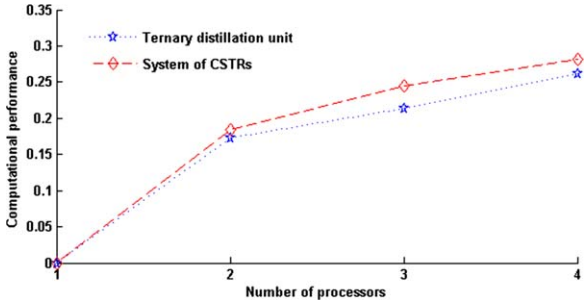

Figure 9. Computational performance of this approach when using multiple cores.

[Color figure can be viewed in the online issue, which is available at wileyonlinelibrary.com].

Due to the limitations on the number of physical cores available, this study was not able to test the computational demands using a larger number of cores. However, it is expected that the optimal number of cores that can be used in this method is directly proportional to the number of worst-case performance outputs that need to be assessed per function evaluation. That is, for the case of the ternary distillation unit, the worst-case performance of 6 outputs is needed to completely evaluate the cost function and the constraints considered in that optimal design and control formulation (see Figure 2). Thus, it is expected that using six physical cores in the complete evaluation of the optimization function will return the optimal CPU time for this system, i.e., using more than 6 cores for that case study may not improve the computational efficiency in the evaluation of the optimization function. The results presented in this study can be used as a guideline to implement this optimal process and control design methodology to other engineering applications.

Conclusions

A new methodology that integrates process synthesis analysis and control structure selection for the optimal design of dynamic systems has been presented. The key feature introduced by this method is the simultaneous evaluation of dynamic flexibility and feasibility for optimal process synthesis and control structure design. Also, computer parallelization techniques can be implemented, which makes this method computationally attractive. Moreover, the norm-bounded formulation used to assess the worst-case increase (or decrease) in the process outputs allows a general description of the disturbances, i.e., disturbances are treated as unmeasured random (stochastic) time-discrete inputs that are bounded by lower and upper limits. Accordingly, the optimal process flowsheet and control structure obtained by this approach is robust since it can accommodate the critical realizations in the disturbances that produce the worst-case performance in the process outputs. Furthermore, a robust stability test based on Quadratic Lyapunov theory is included in this methodology to ensure that the optimal design is asymptotically stable for any of the magnitude-bounded perturbations considered in the analysis.

The methodology presented in this work was used to evaluate the optimal process and control design of a system of CSTRs connected in series and a ternary distillation column. A study on the computational costs using MATLAB revealed that the evaluation of the worst-case performance using this method is at least 24 times more efficient than using a formal dynamic optimization formulation. Also, the computational costs of this method are significantly reduced when the code that implements this simultaneous design and control approach is executed in parallel using multiple processors. Thus, this method is an efficient tool that can be used for optimal process synthesis and control structure design.

Literature Cited

1. Seider WD, Seader JD, Lewin DR. Product and process Design Principles: Synthesis, Analysis and Evaluation. 2nd ed. New York, NY: John Wiley and Sons, Inc; 2004.
2. Grossmann IE, Straub DA. Recent developments in the evaluation and optimization of flexible chemical processes. In: Puigjaner, Espuña, eds. Proceedings of COPE '91. 1991;41.
3. Lenhoff AM, Morari M. Design of resilient processing plants. 1. Process design under consideration of dynamics aspects. *Chem Eng Sci*. 1982:37:245–258.
4. Shinskey FG. Uncontrollable processes and what to do about them. *Hydrocarb Process*. 1983;62:179–182.
5. Luyben WL. The need for simultaneous design education. In: Seferlis P, Georgiadis MC. The Integration of Processes Design and Control. New York, NY: Elsevier; 2004:17:10–41.
6. Seferlis P, Grievink J. Process design and control structure screening based on economic and static controllability criteria. *Comput Chem Eng*. 2001;25:641–647.
7. Palazoglu A, Arkun A. A multiobjetive approach to design Chemical-plants with robust dynamic operability characteristics. *Comput Chem. Eng*. 1986;10:567–575.
8. Palazoglu A, Arkun A. Design of chemical plants with multiregime capabilities and robust dynamic operability characteristics. *Comput Chem Eng*. 1987;11:20–216.
9. Luyben ML, Floudas CA. Analyzing the interaction of design and control. 1. A multiobjetive framework and application to binary distillation synthesis. *Comput Chem Eng*. 1994;18:933–969.
10. Alhammadi A, Romagnoli J. Process design and operation: Incorporating environmental, profitability, heat integration and controllability considerations. In: Seferidis P, Georgiadis MC, eds. The Integration of Process Design and Control. New York, NY: Elsevier; 2004;17: 264–305.
11. Brengel DD, Seider WD. Coordinated design and control optimization of nonlinear processes. *Comput Chem Eng*. 1992;16:861–886.
12. Mohideen MJ, Perkins JD, Pistikopoulos EN. Optimal design of dynamics systems under uncertainty. *AIChE J*. 1996;42:2251–2272.
13. Bansal V, Perkins JD, Pistikopoulos EN, Saraiva PM. A case study in simultaneous design and control using rigorous, mixed-integer dynamic optimization models. *Ind Eng Chem Res*. 2002;41:760–778.
14. Kookos IK, Perkins JD. An algorithm for simultaneous process design and control. *Ind Eng Chem Res*. 2001;40:4079–4088.
15. Bahri PA, Bandoni JA, Romagnoli JA. Integrated flexibility and controllability analysis in design of chemical processes. *AIChE J*. 1997; 43:997–1015.
16. Malcolm A, Polan J, Zhang L, Ogunnaike BA, Linninger AA. Integrating systems design and control using dynamic flexibility analysis. *AIChE J*. 2007;53:2048–2061.
17. Tlacuahuac AF, Biegler LT. Simultaneous mixed-integer dynamic optimization for integrated design and control. *Comput Chem Eng*. 2007;31:588–600.
18. Lopez-Negrete R, Flores-Tlacuahuac A. Integrated design and control using simultaneous mixed integer dynamic optimization approach. *Ind Eng Chem Res*. 2009;48:2605–2615.
19. Moon J, Kim S, Linninger AA. Integrated design and control under uncertainty: Embedded control optimization for plantwide processes. *Comput Chem Eng*. 2011;35:1718–1724.
20. Schweiger CA, Floudas CA. Interaction of design and control: optimization with dynamic models. In: Hager WH, Padarlos PM, eds. Optimal Control. The Netherlands: Kluwer Academic Publishers; 1998:388–435.
21. Baker R, Swartz CLE. Rigorous handling of input saturation in the design of dynamically operable plants. *Ind Eng Chem Res*. 2004;43: 5880–5887.
22. Ricardez Sandoval LA, Budman HM, Douglas PL. Simultaneous design and control of processes under uncertainty: A robust modelling approach. *J Process Control*. 2008;18:735–752.

23. Ricardez-Sandoval LA, Budman HM, Douglas PL. Simultaneous design and control of chemical processes with application to the Tennessee Eastman Process. *J Process Control*. 2009;19:1377–1391.
24. Lee JH, Braatz RD, Morari M, Packard A. Screening tools for robust control structure selection. *Automatica*. 1995;31:229–235.
25. Lu XJ, Li HX, Duan JA, Sun D. Integrated design and control under uncertainty: A fuzzy modeling approach. *Ind Eng Chem Res*. 2010;49:1312–1324.
26. Braatz RD, Lee JH, Morari M, Packard A. Screening tools for robust control structures for uncertainty systems. *Comput Chem Eng*. 1996; 20:463–468.
27. Ricardez-Sandoval LA, Budman HM, Douglas PL. Applications of robust control tools to the simultaneous design and control of dynamic systems. *Ind Eng Chem Res*. 2009;48:801–813.
28. Lu XJ, Li HX, Chen CLP. Robust optimal design with consideration of robust eigenvalue assignment. *Ind Eng Chem Res*. 2010;49:3306–3315.
29. Gerhard J, Marquardt W, Monnigmann M. Normal vectors on critical manifolds for robust design of transient processes in the presence of fast disturbances. *Soc Ind Appl Math*. 2008;7:461–490.
30. Gerhard J, Monnigmann M, Marquardt W. Constructive nonlinear dynamics foundations and application to robust nonlinear control. In: Meurer T, Graichen K, Gilles ED, eds. Control and Observer Design for Nonlinear Finite and Infinite Dimensional Systems, Berlins: Springer-Verlag; 2005:165–182.
31. Monnigmann M, Marquardt W. Steady-state process optimization with guaranteed robust stability and flexibility: Application to HDA reaction section. *Ind Eng Chem Res*. 2005;44:2737–53.
32. Ricardez-Sandoval LA. Optimal design and control of dynamic systems under uncertainty: A probabilistic approach. *Comput Chem Eng*. 2012;43:91–107.
33. Alvarado-Morales M, Abd Hamid MK, Sin G, Gernaey KV, Woodley JM, Gani R. A model-based methodology for simultaneous design and control of a bioethanol production process. *Comput Chem Eng*. 2010;34:2043–2061.
34. Hamid MKA, Sin G, Gani R. Integration of process design and controller design for chemical processes using model-based methodology. *Comput Chem Eng*. 2010;34:683–699.
35. Ramirez E, Gani R. Methodology for the design and analysis of reaction separation systems with recycle. 2. Design and control integration. *Ind Eng Chem Res*. 2007;46:8084–8100.
36. Chawankul N, Ricardez Sandoval LA, Budman H, Douglas PL. Integration of design and control: A robust control approach using MPC. *Can J Chem Eng*. 2007;85:433–446.
37. Sakizlis V, Perkins JD, Pistikopoulos EN. Recent advances in optimization-based simultaneous process and control design. *Comput Chem Eng*. 2004;28:2069–2086.
38. Swartz CLE. The use of controller parametrization in the integration of design and control. In: Seferlis P, Georgiadis MC, eds. The Integration of Process Design and Control. Amsterdam, The Netherlands: Elsevier; 2004:239–263.
39. Francisco M, Vega P, Alvarez H. Robust integrated design of processes with terminal penalty model predictive controllers. *Chem Eng Res Des*. 2011;89:1011–1024.
40. Gutierrez G, Ricardez LA, Budman H, Prada C. Integration of design and control using an MPC-based superstructure for control structure selection. Preprints of the 18th IFAC World Congress, Milan, Italy.2011:7648–7653.
41. Seferlis P, Georgiadis MC. The integration of process design and control. 1st ed. Amsterdam, The Netherlands: Elsevier; 2004.
42. Ricardez-Sandoval LA, Budman H, Douglas P. Integration of design and control for chemical processes: A review of the literature and some recent results. *Ann Rev Con*. 2009;33:158–171.
43. Yuan Z, Chen B, Sin G, Gani R. State-of-the-art and progress in the optimization-based simultaneous design and control for chemical processes. *AIChE J*. 2012;58:1640–1659.
44. Mohideen MJ, Perkins JD, Pistikopoulos EN. Robust stability considerations in optimal design of dynamic systems under uncertainty. *J Process Control*. 1997;7:371–385.
45. Ricardez-Sandoval LA, Budman HM, Douglas PL. Simultaneous design and control: A new approach and comparison with existing methodologies. *Ind Eng Chem Res*. 2010;49:2822–2833.
46. Ricardez-Sandoval LA, Douglas PL, Budman HM. A methodology for the simultaneous design and control of large-scale systems under process parameter uncertainty. *Comput Chem Eng*. 2011;35:307–318.
47. Ljung L. System Identification: Theory for the User. 1st ed. Englewood Cliffs, NJ: Prentice Hall; 1987.
48. Morari M, Zafiriou E. Robust Process Control. Englewood Cliffs, NJ: Prentice Hall; 1989.
49. Skogestad S, Postlethwaite I. Multivariable Feedback Control: Analysis and Design. Hoboken, NJ: John Wiley & Sons, Inc.; 2005.
50. Zhou K, Doyle JC, Glover K. Robust and Optimal Control. Englewood Cliffs, NJ: Prentice Hall; 1996.
51. Slotine JE, Li W. Applied Nonlinear Control, Englewood Cliffs, NJ: Prentice Hall; 1991.
52. Khalil HK. Nonlinear Systems. 3rd ed. Englewood Cliffs, NJ: Prentice Hall; 2002.
53. Boyd S, Yang QP. Structured and simultaneous Lyapunov functions for system stability problems. *Int J Control*. 1989;49:2215–2240.
54. Gahinet P, Nemirovski A, Laub AJ, Chilali M. LMI Control Toolbox, For Use with MATLAB. Natick, MA: The MathWorks, Inc; 1995.
55. Economic Indicators. Chemical Engineering. 2012;119:83–84.
56. Douglas JM. Conceptual Design of Chemical Processes. New York, NY McGraw-Hill; 1988.
57. Shampine LF, Reichelt MW. The MATLAB ODE suite. *Siam J Sci Comput*. 1997;18:1–22.
58. Jones DR. Direct. Encyclopedia of Optimization. Dordrecht, Germany: Kluwer Academic Publishers; 2001.
59. Nocedal J, Wright SJ. Numerical Optimization (Springer Series in Operations Research and Financial Engineering). New York, NY: Springer Verlag; 2006.
60. Parallel Computing Toolbox in MATLAB 5.2. The MathWorks, Inc; 2011.

Manuscript received Sept. 27, 2012, revision received Nov. 29, 2012, and revision received Jan. 29, 2013.